Nanoporous gold: Novel Catalytic and Sensor Applications

Dissertation
zur Erlangung des Doktorgrades
der Naturwissenschaften
- Dr. rer. nat. -

Vorgelegt dem Promotionsausschuss
des Fachbereichs 2 (Chemie/Biologie)
der Universität Bremen
von

Arne Wittstock

Bremen, im April 2010

1. Gutachter: Prof. Dr. Marcus Bäumer (Universität Bremen)

2. Gutachter: PD Dr. Michael Gottfried (Universität Erlangen/Nürnberg)

Hiermit erkläre ich, dass ich die vorliegende Arbeit selbständig angefertigt und keine außer den angegebenen Hilfsmitteln verwendet habe. Diese Arbeit wurde nicht vorher an anderer Stelle eingereicht.

Bremen, den

This thesis is based on the following papers, which will be referred to in the text by their roman numerals:

I) **Nanoporous Au: An Unsupported Pure Gold Catalyst?**
Wittstock, A.; Neumann, B.; Schaefer, A.; Dumbuya, K.; Kübel, C.; Biener, M. M.; Zielasek, V.; Steinrück, H.-P.; Gottfried, J. M.; Biener, J.; Hamza, A.; Bäumer, M
The Journal of Physical Chemistry C, **2009**, 113 (14), 5593-5600,
http://pubs.acs.org/doi/abs/10.1021/jp808185v

II) **Novel nanoporous gold catalysts for green chemistry: selective gas-phase oxidative coupling of methanol at low temperature**
Wittstock, A.; Zielasek, V.; Biener, J.; Friend, C. M.; Bäumer, M
Science, **2010**, 327 (5963), 319-322.
http://www.sciencemag.org/cgi/content/full/327/5963/319

III) **Surface-chemistry-driven actuation in nanoporous gold**
Biener, J.; Wittstock, A.; Zepeda-Ruiz, L. A.; Biener, M. M.; Zielasek, V.; Kramer, D.; Viswanath, R. N.; Weissmuller, J.; Baumer, M.; Hamza, A. V.
Nature Materials **2009,** *8* (1), 47-51
http://www.nature.com/nmat/journal/v8/n1/pdf/nmat2335.pdf

IV) **Surface Chemistry in Nanoscale Materials**
Biener, J.; Wittstock, A.; Baumann, T.; Weissmüller, J.; Bäumer, M.; Hamza, A.
Materials **2009,** *2* (4), 2404-2428
http://www.mdpi.com/1996-1944/2/4/2404/

V) **Effect of surface chemistry on the stability of gold nanostructures**
Biener, J.; Wittstock, A.; Biener, M.M.; Nowitzki, T.; Hamza, A.V.; and Bäumer, M.
Submitted to Langmuir in February 2010

VI) **Ultralow loading Pt nanocatalysts prepared by atomic layer deposition on carbon aerogels**
King, J. S.; Wittstock, A.; Biener, J.; Kucheyev, S. O.; Wang, Y. M.; Baumann, T. F.; Giri, S. K.; Hamza, A. V.; Bäumer, M.; Bent, S. F.
Nano Letters, **2008,** *8* (8), 2405-2409
http://pubs.acs.org/doi/abs/10.1021/nl801299z

Statement regarding my contribution to the published work:

All stated publications are unexceptionally based on the collaboration of several researches.

Nevertheless, for *publication (I)* I was responsible for writing the manuscript, the preparation of samples, and for the catalytic characterization of samples (Björn Neumann as a research student being strongly involved in the experiments).

Regarding *publication (II)* I was strongly involved in writing the manuscript and performed the experimental work.

For *publication (III)* I performed the experimental work and was only to a minor extend involved in the preparation of the manuscript (focus was on artwork).

In case of the review type *publication (IV)* I was responsible for two chapters of the manuscript.

For *publications(V)* I performed the experimental work on the annealing of nanoporous gold and provided some art work to the manuscript.

In *publication (VI)* I performed the catalytic characterization of samples, was involved in the data evaluation (TEM and RBS) and contributed to the preparation of the manuscript.

.

Zusammenfassung

Nanoporöses Gold (np-Au) wurde untersucht hinsichtlich seiner Anwendungen für die heterogene Gasphasenkatalyse sowie seiner Anwendungen in der Aktorik bzw. Sensorik. Darüber hinaus wurde der Einfluss von Adsorbaten auf die Stabilität der mesoporösen Struktur des Goldes untersucht. Neben der zielgerichteten Herstellung des np-Au lag der Schwerpunkt hierbei auf dem Verständnis der chemischen Prozesse an der Oberfläche des Materials.

Nanoporöses Gold kann durch Entlegieren einer Gold-Silber Legierung hergestellt werden. Entlegieren bezeichnet einen Prozess, bei dem selektiv die unedlere Komponente (hier Ag) aus der (bi-) metallischen Legierung fast vollständig herausgelöst wird. Durch Selbststrukturierung entsteht eine selbsttragende mesoporöse Gold-Struktur (> 99 at% Gold), deren Stege und Poren nur wenige zehn Nanometer groß sind. Das hohe Oberflächen-zu-Volumen Verhältnis und die stark gekrümmte Oberfläche der Stege dieses Materials führen zu einzigartigen Materialeigenschaften. So kann CO bereits bei Temperaturen von – 20 °C mit molekularem Sauerstoff oxidiert werden. Bei der Untersuchung von Proben mit unterschiedlich hohen Restsilbergehalten stellte sich in diesem Zusammenhang ein deutlicher Einfluss des Silbers heraus, das nach dem Entlegieren im Material verbleibt. Die beobachtete Charakteristik und die Kinetik der katalysierten Oxidation von CO legen eine entscheidende Rolle des Silbers bei der Aktivierung von molekularem Sauerstoff nahe.

Die schwache Bindung von Adsorbaten auf Goldoberflächen begründet die katalytische Aktivität bei niedrigen Temperaturen, darüber hinaus kann dieser Umstand zum Erzielen besonders hoher Selektivität genutzt werden. Als Beispiel wurde die katalytische Oxidation von Methanol untersucht. Bereits bei 20 °C konnte die Oxidation von Methanol zum Methylformiat durchgeführt werden. Die Selektivität bei dieser Umsetzung lag bei nahezu 100 %. Die thermodynamisch begünstigte Totaloxidation (Verbrennung) zum CO_2 spielte nur eine untergeordnete Rolle, auch bei erhöhtem Umsatz bei 80 °C Reaktionstemperatur machte diese weniger als 3 % des Gesamtumsatzes aus. Die Reaktivität und der Mechanismus der Oberflächenreaktion, insbesondere der Umstand, dass ausschließlich der Ester gebildet wurde, können auf der Grundlage von Modellexperimenten unter UHV Bedingungen verstanden werden. Lediglich die Aktivierung des molekularen Sauerstoffs kann nicht auf die Aktivität des Goldes allein zurückgeführt werden. Jedoch auch hier stellte sich ein deutlicher Einfluss des Silbers heraus, der auf die Aktivierung des molekularen Sauerstoffs zurückzuführen ist.

Das hohe Oberflächen-zu-Volumen Verhältnis von np-Au eröffnet neben der Katalyse viele weitere Anwendungsfelder. So ist der Oberflächenstress von Metallen durch die Adsorption von Substanzen beeinflussbar. Im Falle von np-Au kann der hohe Anteil der Oberfläche am Gesamtmaterial zu einer Beeinflussung der gesamten Materialeigenschaften führen. Die Adsorption von atomarem Sauerstoff (O_{ads}) verdeutlicht dieses beispielhaft. Aufgrund der geringen Dissoziationsrate von molekularem Sauerstoff wurde Ozon als Quelle für atomar auf der Oberfläche adsorbierten Sauerstoff gewählt. Die Bedeckung der Oberfläche des np-Au mit O_{ads} durch Ozon Exposition bzw. dessen Entfernung durch Exposition von Kohlenmonoxid führte zu makroskopisch detektierbaren reversiblen Schrumpfen bzw. Dehnung des Materials von bis zu 0.5 % der Seitenlänge. Dies ist ein Wert, der vergleichbar mit kommerziell erhältlichen Piezo-Keramiken ist. Die Möglichkeit, chemische Energie direkt in mechanische Arbeit umzusetzen, ohne vorher elektrische Energie zu produzieren, stellt ein neuartiges Aktuator-Konzept dar und kann ebenfalls für sensorische Zwecke genutzt werden.

Ein weiterer wichtiger Aspekt der Oberflächenchemie bzw. der Adsorbate ist ihre Rolle für die Stabilisierung der Nanostruktur und dessen gezielte Variation. Die Instabilität und Vergröberung der Strukturen ist durch die stark gekrümmte Oberfläche der Stege und die Oberflächendiffusion der Goldatome bedingt. Diese ist stark von der Temperatur abhängig und kann genutzt werden, um die Strukturen durch Tempern bei Temperaturen oberhalb von 150 °C zu vergröbern. Ein entscheidender Parameter hierbei ist der Einfluss der Adsorbate auf die Diffusionsgeschwindigkeit der Oberflächenatome und somit auf die Stabilität der Struktur. Als Beispiel wurde wiederum die Bedeckung der Oberfläche mit atomarem Sauerstoff durch Exposition mit Ozon gewählt. Proben, die unter einer ozonhaltigen Atmosphäre getempert wurden zeigten unterhalb von 500 K eine deutlich erhöhte Strukturstabilität. Im Vergleich zu den unter einer Inertgasatmosphäre (He) getemperten Proben, deren Stege auf die doppelte Größe anwuchsen, blieben die durch Sauerstoff stabilisierten Stege in ihrer Größe unverändert. Des Weiteren können durch Ausnutzung des limitierten Stofftransportes in die Poren des Materials gezielt Gradienten der Poren- und Steggrößen erreicht werden. Das Konzept der adsorbat-induzierten Strukturkontrolle unterstreicht den Einfluss der Oberfläche und der Chemie an dieser auf die Materialeigenschaften.

Content

1 Introduction

New materials are sought for applications in catalysis, sensing, optics, electronics and other emerging fields. With the event of nanotechnology, innovations greatly profit from the access to new nano-sized materials with novel properties of materials simply resulting from the reduction of size. As a function of size, the chemical, optical, and mechanical behaviour can be tuned allowing adapting the materials specifically to their application. In recent years the field of such "nano-materials" steadily grew. Examples reflecting their technological importance are nano-particles in catalysis, ultra thin films in semiconductor technology or porous materials, such as metal organic frameworks for energy storage. The ultimate aim is to structure and design materials for a specific purpose on the scale of a few atoms.

The length scale determines the electronic, catalytic, optical, and mechanical properties. An example is gold. Despite or due to its value and stability the technological application of gold was for a long time mainly restricted to electrically conductive coatings for electronics, optical coatings, or brazing alloys.(*1*) However, when in the form of nano-particles with diameters of less than 5 nm gold can show remarkable activity for catalytic applications. This fact was first reported by Haruta and Hutchings in the middle 80th last century.(*2-3*) Today, gold catalysis is on the very verge to commercial catalytic application.(*4*)

This effect is based on the reduced length scale of nano particles. One reason is the effect of length scale on the surface to volume (S/V) ratio. For example, the S/V ratio of a sphere with a radius of 1 m increases by nine orders of magnitude when the radius is reduced to 1 nm. Hence, when going from "macro" to "nano" several orders of magnitude are crossed. Materials on the nano scale are to a large extent governed by their surface properties. The surface of a material is an interface and atoms at this interface are in a different electronic (chemical) state, owing to their lower coordination than within the bulk.

Accordingly, monolithic nanoporous materials recently attracted considerable interest. Examples, are aerogels (*5*), metal organic frameworks (*6*), ceramics (*7*), and nanoporous metals (*5, 7-8*). The latter group certainly stands for a particularly interesting class of materials in the context of catalysis, electronics, and optics. Today, different metals, such as Pt, Pd, Au, Ag, Cu etc. are available in a nanoporous form (*8*), thus opening the door for a variety of applications.

In this thesis I will demonstrate that nanoporous gold follows this trend. It is this delicate balance between gold's inertness and surface related phenomena which creates a range of new and beforehand unseen applications. I will discuss the surface chemistry of np-Au in terms of catalytic activity and selectivity; this is the impact of surface chemistry on the surrounding gases. In addition, I will discuss the influence of surface chemistry on the surface stress and mobility e.g. surface diffusion of surface atoms; this is the impact of surface chemistry on the material itself. We will see that:

- np-Au exhibits remarkable catalytic activity for oxidation reactions at low temperatures such as the oxidation of CO and methanol, for example
- selectivity close to 100 % can be achieved for the oxidation of methanol when using np-Au. This example shows that high selectivity and durability can be achieved taking advantage of the relatively weak interaction of molecules with gold surfaces
- the surface chemistry of np-Au correlates with that of pure (i.e. single crystalline) gold surfaces. Reactivity and selectivity can be anticipated based on mechanistic understanding of reactivity making np-Au a predictable catalyst
- (local) tuning of surface properties by residual Ag regulates availability of active oxygen and thus the oxidative power of the material can be tuned
- the surface chemistry can lead to a change of surface stress. In case of np-Au which is distinguished by its high surface to volume (S/V) ratio this effect can lead to a macroscopic strain response of up to 0.5 %.
- the structure of np-Au can be tuned for a specific use. Taking advantage of surface chemistry i.e. bonding of adsorbates such as oxygen the structure can be stabilized or even gradients can be induced

2 Nanoporous Gold

Nanoporous gold is generated by dealloying of a gold alloy containing a less noble constituent such as silver or copper. The dealloying process by itself is an ancient technology and was already used by the Incan people some hundred years ago. They dealloyed (etched) and glazed the surface of a gold-copper alloy giving the illusion of shining bulk gold. This technique called depletion gilding (*mis-en-colour*) was used throughout the centuries in Europe, too.(*9-12*)

The recent focus on "nano" and the development of sophisticated microscopical techniques such as electron microscopy since the middle of the last century shifted the focus on dealloying techniques from corrosion studies towards the material science. Since the 1960s Pickering and Swann investigated the corrosion of Au alloys, presenting first transmission electron micrographs (TEMs) revealing the porous morphology of np-Au. (*13-14*) Later in 1979 Forty and co-workers were able to obtain TEMs of monolithic np-Au generated by etching of a Ag-Au alloy in nitric acid.(*12, 15*) These images proved the 3 dimensional porous structure of np-Au in the range of only some tens of nanometers.

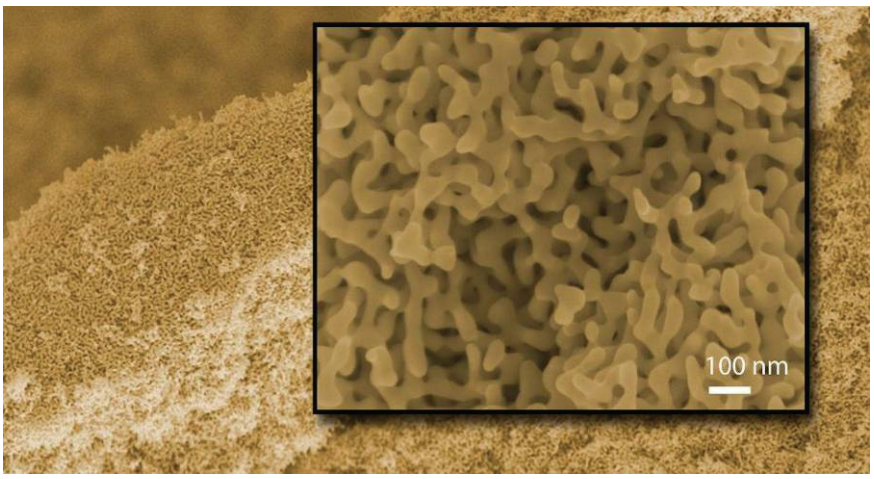

Figure 1: SEM showing the 3 dimensional structure of np-Au generated by etching of a Au-Ag alloy by concentrated nitric acid. The resulting structure can be characterized as (open-cell) metal foam with ligaments and pores in the range of a few tens of nanometers.

In recent years the number of publications concerning nanoporous gold steadily increased by about 30 percent per year, from 11 publications in 2001 to more than 100 publications in the year 2009 (ISI Web of Knowledge). Today, nanoporous gold is used in the field of catalysis, sensors, actuators, optics, and many more. First review articles appearing in 2009 provided an overview about the various aspects of nanoporous gold. (*5, 7, 16-17*) The interdisciplinary nature of this material ranging from its outstanding material properties to surface chemistry related phenomena poses a challenge when describing and explaining its exceptional properties. Here, we will discuss np-Au and its potential uses from the perspective of surface chemistry and surface induced phenomena. In the chapters 4 and 5 we will further discuss the impact of surface chemistry on mechanical properties.

2.1 Creating nanoporosity

The starting compounds for the generation of np-Au are intermetallics of gold, containing at least one less noble metal. Most prominent materials are the alloys of Au-Ag (*10, 12*), Au-Cu (*18-19*), and Au-Al (*8, 20*). All three starting materials can be processed resulting in a porous and monolithic gold material. The dealloying procedure and the resulting material though differ with respect to porosity and composition. The reason lies within the different phase behaviour of the various intermetallics and the different tendency to passivate during the dealloying procedure. For example, the intermetallics of Au and Al (Al_2Au, AlAu) show different characteristics during etching (*21*). Most importantly, Al and Cu tend to passivate during dealloying leading to incomplete leaching in the order of more than 20 at% residual Al and Cu within the np-Au, respectively.(*8, 18, 20*) On the contrary, the alloy of Au and Ag is a so called "solid solution" and solidifies in just one fcc crystal phase, regardless of the composition of the alloy, and can be de-alloyed to > 99 percent.(*1, 22*) The resulting porous structure of the np-Au is homogenous throughout the entire material. When dealing with np-Au it is commonly generated from a Au-Ag alloy owing to the obvious advantages of this preparation route.

The driving force for dealloying is the difference in standard potential ΔE of the constituents A and B as described by the change of the free enthalpy ΔG which is a function of the standard potential ΔE^0 and the molar fraction x of the particular component A and B[1] (additional parameters are the universal gas constant R, the temperature T, the number of electrons transferred z and the Faraday constant F):

$$\Delta G_A = \Delta G_A^0 - RT\ln(x_A) \Leftrightarrow \Delta E_A = \Delta E_A^0 - \frac{RT}{zF}\ln(x_A) \qquad \text{(equ. 1a)}$$

and

$$\Delta G_B = \Delta G_B^0 - RT\ln(x_B) \Leftrightarrow \Delta E_B = \Delta E_B^0 - \frac{RT}{zF}\ln(x_B)\,. \qquad \text{(equ. 1b)}$$

Accordingly, the driving force (potential ΔE) can be expressed by:

$$\Delta E^{dealloying} = \Delta E_A - \Delta E_B = \Delta E_{AB}^0 - \frac{RT}{zF}\ln(\frac{x_A}{x_B}) \qquad \text{(equ. 2)}$$

It is thus the different electrochemical potential of both constituents which is the prerequisite for the dealloying procedure. In this context the component A is the nobler component, such as Au, and the component B is the less noble component, such as Ag.

[1] The activity of the particular component within the surrounding electrolyte is assumed to be negligible small i.e. zero

However, it is also clear that the fraction of the less noble constituent cannot become zero and the dealloying *cannot proceed to 100 %.*

Besides thermodynamic considerations two additional parameters are essential for de-alloying, the so called "parting limit" (*23-24*) and the "critical potential" (*25-27*). Only alloys of a certain range of composition can be dealloyed. The fact that for example the fraction of Ag in the starting alloy has to be more than 55 at% is a consequence of the so called parting limit. For lower fractions of Ag the dealloying does not proceed. This effect can be understood in terms of a coordination effect; for low Ag fractions within the material the coordination by Au atoms increases. A high coordination leads to passivation of the particular atom. Artymowicz et al. recently presented a kinetic Monte-Carlo simulation including percolation theory.(*28*) They showed that the coordination threshold of 9 leads to the experimentally found parting limit of about 55 at%.

Another parameter for de-alloying is the so called critical potential (E_c). This effect can be understood on the bases of the commonly known over-potential in electrochemistry. The theoretical potential as described in equ. 2 does not suffice to induce bulk corrosion. The kinetics i.e. the activation barrier for surface diffusion of the more noble Au atoms prevents corrosion throughout the bulk material. Hence, only at a certain potential (higher than the thermodynamic threshold) the current that is the dissolution of Ag atoms rapidly increases. This potential E_c depends on the composition of the starting alloy, the electrolyte, and further additives like halides.(*25-27*)

None of these parameters can solely explain the formation of a 3-dimensional sponge-like morphology. Different theories based on atomistic models of dealloying have been proposed; Erlebacher and co-workers presented a model which reproduces the morphology of np-Au. (*7, 29-30*) This model is based on three competing processes, the electrochemical dissolution of the less noble constituent (Ag), the surface diffusion of the noble constituent (Au), and capillary action.(*7, 30*) A schematic drawing of the mechanism is shown in Figure 2. While the Ag atoms are dissolved in a layer-by-layer fashion, the gold atoms can diffuse along the surface and form islands. Further dissolution of Ag atoms leads to erosion of islands so that ligaments are formed. On the basis of that rather simple model trends in de-alloying characteristics can be satisfactorily explained as for example the tendency to form larger ligaments when halides are added to the electrolyte during dealloying (*27*) or smaller ligaments are formed when the temperature is lowered (*31*). Both parameters affect the mobility of the gold atoms and thus the size of islands which are initially formed by surface diffusion.

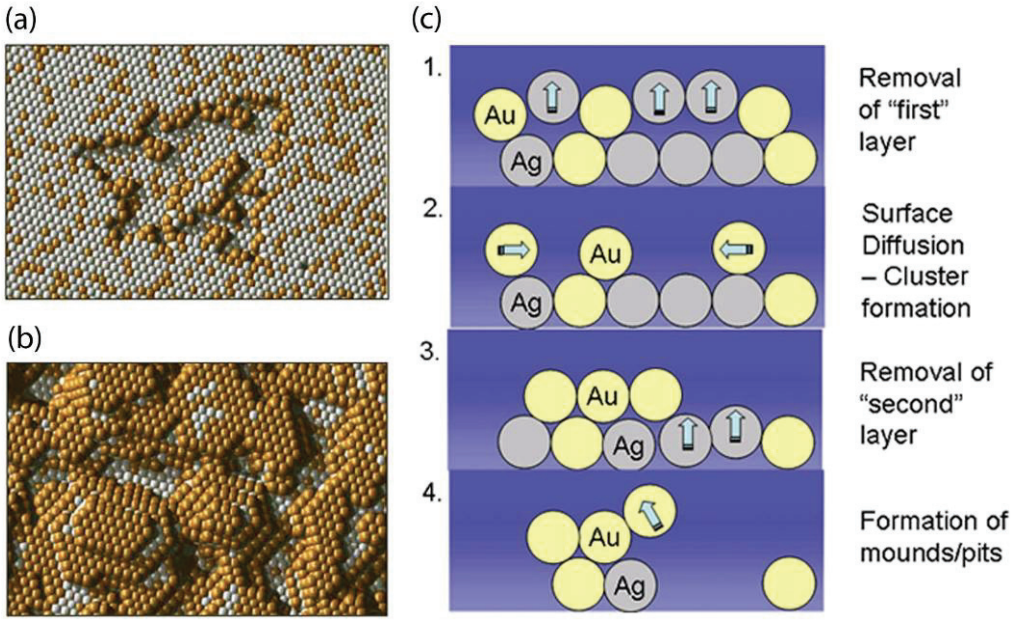

Figure 2: Atomistic model of de-alloying for a fcc gold-silver alloy (sections (a) and (b) reproduced from ref. (7)). The sections (a) and (b) show illustrations from a kinetic Monte Carlo simulation, the greyish Ag atoms are dissolved in a layer by layer fashion. The diffusion of the Au atoms along the surface leads to formation of islands, as can be seen in section (b). Single steps of the dealloying mechanism are depicted in section (c).

2.2 Surface-porosity related phenomenon

When dealing with "nano" sized materials new material properties and applications are discussed and found.(*5, 7*) But why and to what extend should a material such as gold "change" when becoming nano-sized? The reason lies within the reduced characteristic length and the increased surface[2] to volume ratio of the objects. When moving from objects with characteristic length-scales (e.g. diameter, edge length) in the order of centimetres or millimetres to the nanometer scale, the surface to volume ratio is increased by a factor of more than one million. Accordingly, nanosized object are to a large extend determined by their surface chemical properties. In the following, two effects which are related to surfaces and low coordination of atoms are exemplarily discussed.

The charge redistribution due to low coordination of surface atoms gives rise to surface stress.(*32-36*) The excess charge from unsaturated bonds is redistributed into in-plane bonds which are strengthened or weekend, depending on whether the additional charge is distributed into bonding or antibonding states. Compared to bond length of atoms within the bulk the distance between surface atoms can thus be altered leading to surface stress. For compressive stress the surface tends to expand compared to the bulk whereas for tensile stress the surface tends to shrink.(*34*) A typical consequence of surface stress is a reconstruction of the surface. Giving an example, the Au(111) surface reconstructs in the

[2] The term surface is used with the same meaning as the term interface. In reality, surfaces are always interfaces.

commonly known Herringbone reconstruction.(*37-38*) The tensile surface stress of the Au(111) surface is compensated by incorporation of about 4 % additional atoms into the surface as compared to the bulk. Recently, several investigations showed that in case of nanoporous metals (np-Au, np-Pt) a change of surface stress can lead to macroscopically detectable strain of the entire material, an effect formerly known only for piezo ceramics.(*32-33, 39-40*)

An additional effect is exploited in catalysis. The low coordination of surface atoms enhances the reactivity of (metal) surfaces. The desorption enthalpy of CO on gold surfaces is (amongst others) a function of the roughness that is the coordination number of surface atoms.(*41*) In general there are two ways in which the coordination of a surface atom can influence the interaction with adsorbates, one is electronic (adsorption enthalpy) and the other one is geometric (activation barrier), in reality both effects are hardly separated. The concept of d-band centre was first introduced from Norskov for the description of electronic effects on the interaction of gases with metallic surfaces.(*42*) The d-band centre is defined as the first moment of the density of d-states. The position of the d-band centre with respect to the Fermi level affects the ability of a metal surface atom to form a bond with an adsorbate. For example, transition metals tend to have higher d-states in case of low coordination numbers (kink-, edge-sites). Owing to this fact these atoms interact more strongly with adsorbates than atoms in a closed packed surface.(*43*) Additionally, the geometry of the substrate provides specific adsorption sites which play a crucial role for activation of adsorbed molecules (lowering the activation barrier).(*44*) Both effects contribute to the catalytic performance of a metal. In case of gold the role of low coordination even determines whether the surface shows any catalytic activity.(*45*)

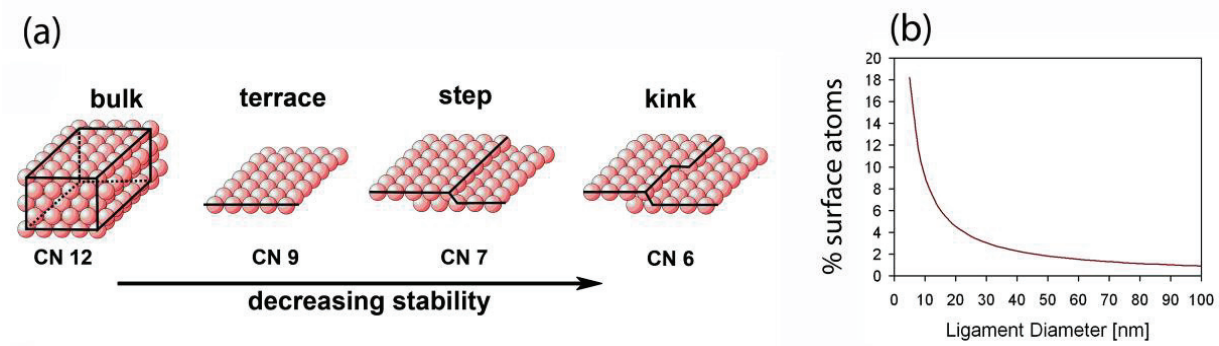

Figure 3: (a) The coordination of atoms depends on their location. In general, the stability of atoms decreases with the coordination number (CN) (image courtesy of J. Biener). (b) The fraction of surface atoms rapidly increases when the characteristic length is decreased. This is exemplary shown for a straight ligament (pillar) (numbers are based on a geometric consideration)

3 Catalysis by nanoporous gold

The first experimental results regarding the catalytic potential of np-Au were published in 2006 by Bäumer and co-workers (*46*) and only a short period of time later by Ding and co-workers (*47*). They investigated the catalytic oxidation of carbon monoxide (CO) with molecular oxygen (O_2). Both groups detected independently high catalytic activity at temperatures even below 0 °C. This finding was spectacular and unexpected so far, since all previous catalytically active[3] gold catalysts were comprised of nanoparticles on a reducible support, such as TiO_2.(*48-49*) Not only is nanoporous gold catalytically active without any oxidic (reducible) support material but also the size of the ligaments (30 to 40 nm) is about ten times higher than the upper size limit of 5 nm, which is found to be essential for high catalytic activity of nanoparticles. (*48-49*)

In the meantime, additional catalytic applications of np-Au evolved, such as for example, the liquid phase oxidation of glucose (*50*), the electro-oxidation of methanol (*51-52*) or oxygen reduction reaction like in fuel cell application. (*53-54*) Yet, the presented work on the gas-phase oxidative coupling of methanol (*22*) is the first work showing the potential of np-Au as a catalyst for more complex gas-phase reactions.

The origin of the catalytic activity, especially the activation of molecular oxygen remained a matter of discussion. Only recently Ding et al. repeatedly argued that low coordinated gold surface atoms are the source for activated molecular oxygen.(*16*) However, in the following we will see that most part of the surface chemistry of np-Au can be explained by that of pure gold, while small quantities of Ag remaining within the material after dealloying play a crucial role for the activation of molecular oxygen.

[3] With respect to heterogeneous (gas-solid) reactions

3.1 Kinetics of CO oxidation and the influence of residual Ag

(Relevant papers: I & IV)

The catalytic oxidation of CO with molecular oxygen is a relevant reaction from an application as well as from a mechanistic point of view. The oxidation of harmful CO to the nonhazardous CO_2 plays an important role in exhaust gas cleaning (e.g. in car catalysts). The superior activity of gold for low temperature oxidation of CO and hydrocarbons compared to typical metals used in car catalysts (Pt, Pd, Rh) initiated intense research efforts.(*55-57*) Today, first commercial catalysts are available (NS Gold^{TM} from Nanostella Inc.). Additionally, the selectivity of gold to selectively oxidize CO in the presence of H_2 gives rise to application in hydrogen fuel cells.(*58*) Besides its commercial potential, the oxidation of CO was widely used for investigations of the surface chemistry for example under ultra high vacuum (UHV) conditions. Due to its widespread use it is also dubbed as the "fruit fly" of surface chemistry. Especially, the comparatively simple geometry of the CO molecule, the fact that only one product (CO_2) can be formed, and the detection/surveillance by IR spectroscopy renders the CO oxidation particularly useful to determine and asses fundamental reactivity of surfaces for oxidation reactions.

For these reasons, the CO oxidation was chosen as a first test reaction to investigate the catalytic activity of np-Au . Disks of np-Au (300 μm thick and 4.8 mm in diameter) were investigated under continuous flow conditions (details see ref. (*59*)). To activate the sample, it was held under elevated temperatures (> 60 °C) under a gas stream containing CO and O_2. After 2 to 3 hours the activity steadily increased and eventually reached a steady state. The fact that no activation could be obtained when no CO was present points towards a reaction as the case may be reduction of the surface which leads to the catalytically active state. On the other hand when samples were stored for a longer period of time (several weeks) longer activation periods were necessary, an observation which implies a concurrent cleaning procedure. However, x-ray photoelectron spectroscopy (XPS) at the outer surface of the disks did not reveal a distinct change of chemical state of Au and Ag, respectively, after and before activation. The transfer of the samples from the reactor into the UHV chamber as well as the fact that inherently only the very outer surface of the sample can be investigated by XPS renders this technique difficult to asses the active state of the catalyst surface.

After activation of the sample the catalytic performance was investigated in two ways:

- Catalytic activity as a function of the partial pressure of one reactant
- The overall catalytic activity under stoichiometric conditions ($CO:O_2$ is 2:1)

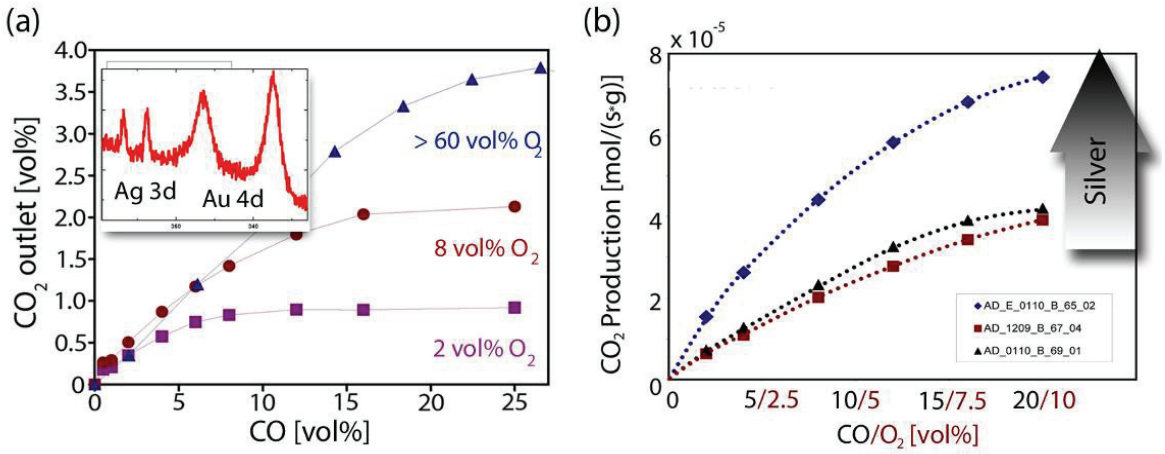

Figure 4: Catalytic activity of np-Au: The oxidation of CO with molecular oxygen at 40 °C. In section (a) the production of CO_2 increases with the supply of CO and O_2 but is eventually limited by oxygen supply. The inset: XP spectrum of the Au 4d and Ag 3d region proving the presence of Ag on the surface of the catalyst. (b) Activity of samples containing different amounts of residual silver (Ag contents were determined by AAS). The reactants were supplied in a stoichiometric ratio of 2:1 ($CO:O_2$). For elevated Ag contents (here 11.4 at% (blue diamonds)) the catalytic activity is increased by nearly a factor of two as compared to samples containing 0.6 at% (red squares) and 0.7 at% res. Ag (black triangles), respectively.

Exemplarily, the conversion as a function of the CO partial pressure for different fixed oxygen partial pressures is shown in Figure 4 (a). In general, the conversion increased with increasing supply of reactants. No poisoning by either reactant was observed. This fact points towards the absence of competition for adsorption on the surface of the catalyst which implies that the interaction with the surface is weak (low surface coverage) and most importantly the adsorption sites for CO and O_2 may be different.

To compare and assess the overall catalytic activity of different samples, in particular with respect to the content of residual silver, the reactants were supplied in a stoichiometric ratio. As expected, the activity increased with increasing supply of reactants (see Figure 4 (b)). However, the production of CO_2 could be considerably increased when samples were prepared containing higher fractions of residual Ag e.g. up to 11 at%. This indicates that (a) Ag plays a role in the catalytic cycle and (b) its presence is beneficial in case of the oxidation of CO.

In order to determine the kinetic parameters of the reaction double logarithmic plots of the activity as a function of the partial pressure where drawn (see Figure 5). The apparent reaction order of O_2 was found to be close to 0.5 for all investigated samples, while the reaction order of CO_2 varied between 0.7 and 1. When taking mass transport phenomena into account (*59-60*) this corresponds to an actual reaction order of 0 for O_2 and between ~ 0 and 1 for CO. These numbers reflect the interaction of the reactants with the catalyst surface. A reaction order of zero implies a fast saturation of adsorption sites for oxygen, either owing

to strong interaction (large adsorption enthalpy) or a very limited number of active sites. On the other hand a reaction order close to 1 as was measured for CO, inflicts that the adsorption i.e. the supply of CO from the gas phase is rate limiting, either because of a weak interaction (low adsorption enthalpy) or a large number of available sites for adsorption. However, with respect to different amounts of Ag within the material no substantial change in the kinetics was observed. This in turn implies that even though the overall activity is altered for increasing amounts of residual Ag the reaction mechanism is not noticeably changed.

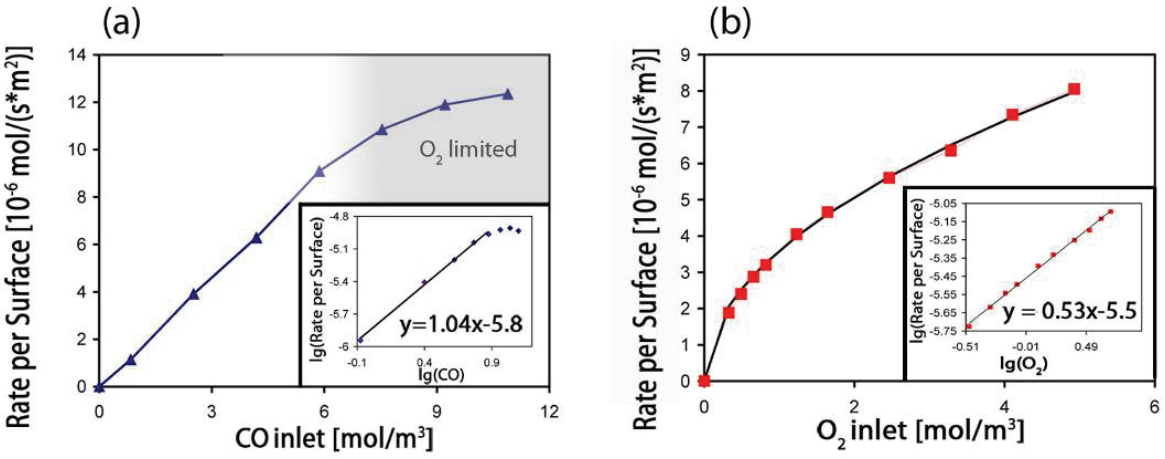

Figure 5: Kinetics of CO oxidation with np-Au. The partial pressure of the particular reactant was varied under an excess of the co-reactant. A double logarithmic plot reveals the exponent i.e. reaction order of the particular component.

The reactivity of gold and silver surfaces regarding CO and O_2 was intensively investigated under ultra high vacuum conditions (UHV).(*38, 41, 61-72*) In general, the desorption enthalpies of CO on Au single crystal surfaces are higher than those on Ag surfaces (see Table 1). This picture is reversed in case of the adsorption of molecular oxygen. On Au surfaces molecular oxygen is only physisorbed (desorption well below 100 K) and no dissociation is observed (*62*). The adsorption of molecular oxygen on Ag is considerably stronger and dissociation is observed.(*72*)

Table 1: Desorption enthalpy of CO and O_2 on Gold and Silver single crystals.

	CO [kJ/mol]	***O_2*** [kJ/mol]	Reference
Au(111) , sputtered Au(111)	44-56	11	(*41, 61-62, 65*)
Ag(111), Ag(110)	27	20-30	(*71-73*)

Our findings are in line with investigations using bimetallic particles. Haruta et al. showed that even small quantities of Ag in the range of 1 at% within a bimetallic Au-Ag catalyst have an impact in the catalytic oxidation of CO.(*74-75*) Although the detailed mechanism and the nature of the active site in these bimetallic catalysts remain a matter of discussion, the activation and adsorption of oxygen is usually ascribed to Ag while the adsorption of CO

is ascribed to Au sites.(*76-79*) This picture fits to our experimental finding, the fast saturation of the surface sites by oxygen (reaction order of zero) is well compatible with the fact that Ag is only the minority on the surface of np-Au. The major part of the surface consists of Au, this may very well offer a large enough number of surface sites so that the supply of CO by the gas phase is rate limiting and thus the reaction order is well above zero, as the case may be even 1.

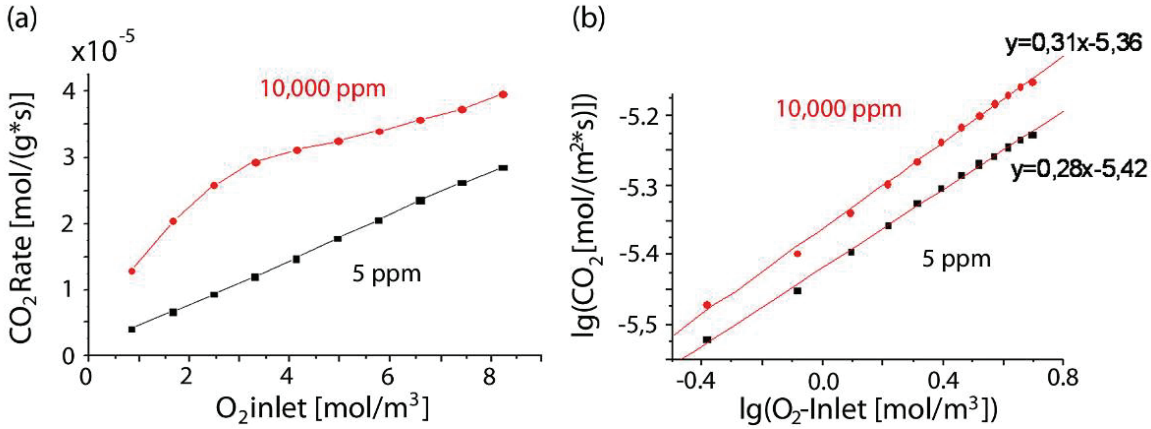

Figure 6: (a) Influence of water on the rate of formation of CO_2. By adding water to the gas stream the catalytic conversion can be enhanced by more than 100 %. The reactant gases were adjusted to a stoichiometric ratio (O_2/CO, 1:2, temperature 20 °C). A water content of 5 ppm is typical for dry reactant gases as supplied from the manufacturer; 10,000 ppm corresonends to 0.01 vol% (~0.4 % rel. humidity). (b) Double logarithmic plot revealing the apparent reaction order (here for O_2). The reaction order is apparently unaltered (at 20 °C, CO > 90 vol%).

An experiment further highlighting the surface chemistry of np-Au is the influence of additives such as water on the catalytic conversion. Water does only weakly adsorb on metal surfaces, especially on Au surfaces. Only if oxygen is present, the water molecule can be activated to transiently form OH species.(*80*) This effect is discussed to have an impact on the activity of surface bonded oxygen, as the case may be by disrupting the oxygen layer which leads to higher activity.(*67*) In case of supported gold catalysts water can amplify the reaction rate by orders of magnitude.(*81*) Here, it is however mostly the interaction with the oxidic support (such as TiO_2) which causes this effect.(*82-83*) In case of catalysis with np-Au and stoichiometric supply of reactants the conversion of CO was increases by about 100 % just by adding 0.01 vol% water to the gas stream (Figure 6 (a)). Neither the apparent reaction orders nor the activation energy was altered when increasing the water content in the gas stream (Figure 6 (b)). When no oxygen was present, the reaction immediately ceased, accordingly, water is not an additional source for oxygen. This finding implies that water works as a co-catalyst; it is not consumed in the process as it is not contained in the products or educts. Nevertheless, it amplifies the total activity of the catalyst. These experimental results are compatible with the observed reactivity of Au surfaces (*80, 84*) and prove that support free metal catalysts working under ambient conditions are influenced by moisture as well.

3.2 Gas phase oxidative coupling of methanol

(Relevant papers: II & IV)

Besides the activity of gold to catalyze oxidation reactions already at low temperatures an additional potential lies in the field of selectivity. The selectivity of a catalyst refers to its ability to preferentially form the desired product among other possible products. Increasing selectivity promotes the effective use of resources and lowers the energy consumption. Not only the economic viability of a catalyst depends on its selectivity but also the ecological viability of the particular process. Today, the ever increasing demand for "greener" technologies further intensifies the research towards selective and nonhazardous catalysts, working under mild conditions with abundant, cheap, and environmental friendly reactants.(*85-89*) Gold is handled as one of the most promising catalyst materials in this respect.(*22, 90-95*)

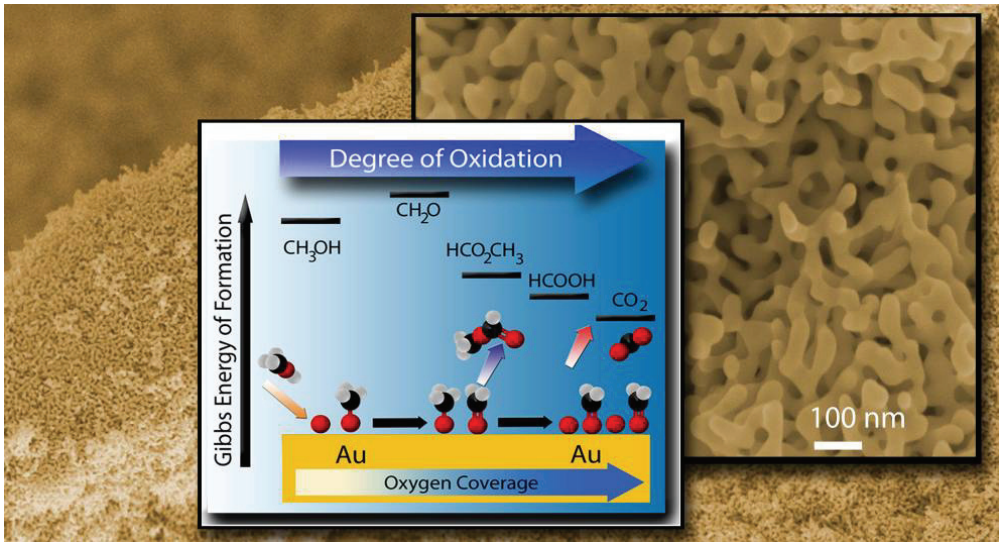

Figure 7: Scanning electron micrographs of np-Au showing its sponge-like structure. Reactant gases can diffuse from the outer surface through the porous structure so that the entire gold surface is available for reaction. Inset (middle): The thermodynamics of methanol oxidation. The total oxidation i.e. production of CO_2 is energetically favoured. The selectivity on gold surfaces is a function of the oxygen coverage.(96)

The selective oxidation of methanol is an exemplary reaction with great industrial relevance. Methanol is the "simplest" alcohol because it contains only one carbon atom (C1). It is the starting compound for a variety of bulk chemicals such as higher alcohols and hydrocarbons, acids and esters.(*97*) Most prominent bulk chemicals derived from methanol are methyl formate, an intermediate for the production of formic acid, and formamide, both of them being produced in the range of several hundred thousand tons per year.(*98-99*) The challenge using catalysis is to selectively produce these various chemicals with carbon in different oxidation states. In terms of thermodynamics the undesired total oxidation that is the formation of CO_2 is strongly favoured (see Figure 7). Selectivity can be induced by slowing down, as the case may be ceasing the oxidation reaction at a certain intermediate, for example by desorption of the particular intermediate before it is further oxidized. The

weak interaction (low adsorption enthalpies) of methanol and its oxidation products on gold (E_{ads} < 21 kcal/mol (*96*)) renders gold surfaces particularly interesting as catalysts for this type of reaction. As np-Au exhibits a large gold surface and thus a large fraction of highly active low coordinated surface atoms it is a promising candidate for the selective oxidation of methanol.

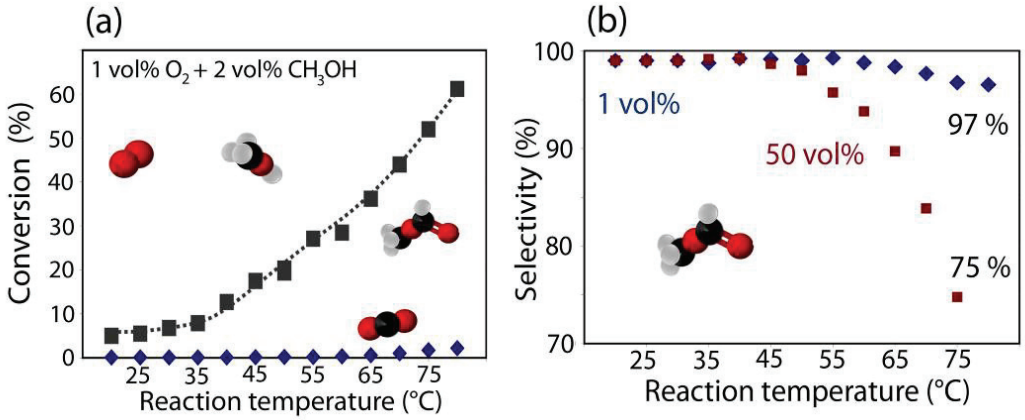

Figure 8: Selective oxidative coupling of methanol to methyl formate using np-Au as catalyst. (a) The production of methyl formate (gray squares) increases with temperature. At 80 °C more than 60 vol% methanol are converted to methyl formate. The total oxidation to CO_2 (blue diamonds) is hardly detectable. (b) The selectivity towards methyl formate production decreases for higher temperatures and oxygen partial pressures. For low oxygen content (1 vol%) the selectivity remains close to 100 %, even for maximal conversion, though.

The investigation of the gas-phase oxidation of methanol with np-Au using molecular oxygen revealed remarkable activity (for details see ref. (*22*)). The methanol is selectively oxidized to the particular ester, the methyl formate (see Figure 8). The reaction already proceeds at 20 °C with nearly 100 % selectivity; the undesired side product CO_2 is hardly detectable. When raising the temperature to 80 °C the conversion can be increased to more than 60 % of methanol, the selectivity however is still at about 97 %. The finding that the selectivity more strongly decreased with temperature for higher oxygen partial pressures is in line with the fact that (a) the activation barrier for the formation of CO_2 is higher (*96*) and (b) that the formation of CO_2 is promoted with increasing oxygen surface coverage (*96*).

According to experiments on Au(111) single crystals the surface is activated by chemisorbed atomic oxygen.(*96, 100-101*) In a Brønstedt-type reaction the methanol reacts with surface oxygen and is subsequently bonded as methoxy on the gold surface. Further, deprotonation leads to the formation of a surface bonded aldehyde. In case of gold this aldehyde is highly reactive, and guides the selectivity towards the methyl formate by a coupling reaction with co-adsorbed methoxy. On the contray, elimination of a hydrogen atom from the aldehyde leads to production of CO_2. It is thus the activation of the gold surface by atomic oxygen, the high reactivity of the surface bonded aldehyde, and the low desorption barrier for methyl formate which inflicts the observed reactivity with np-Au.

To further elucidate the correlation between the molecular model derived from UHV experiments and the observed reactivity under ambient conditions a series of experiments was conducted where a different aldehyde was co-dosed to the reaction mixture. In order to distinguish between formaldehyde which might be generated from reacting methanol, a different aldehyde, i.e., acetaldehyde, was used for this particular experiment. As expected from the molecular model, the selectivity is driven by the activity of the aldehyde. Instead of methyl formate only methyl acetate, the coupling product between the co-dosed aldehyde and methanol was formed. This interesting coupling chemistry was also observed for a variety of different aldehydes with methanol. (*100*)

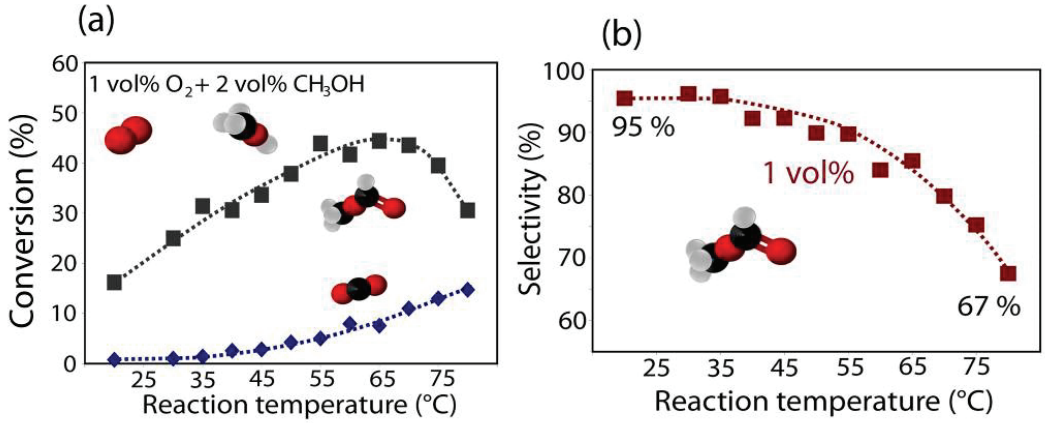

Figure 9: Observed selectivity and catalytic activity when using np-Au samples with higher content of residual silver (here, 2.5 at% Ag). (a) Conversion of methanol to methyl formate (grey squares) and CO_2 (blue diamonds) as a function of the reaction temperature. The conversion to methyl formate exhibits a maximum at ~ 65 °C while production of CO_2 is continuously increasing with temperature. (b) The selectivity towards methyl formate production decreases with temperature and resembles that of sample containing below 1 at% res. Ag at higher oxygen partial pressures (e.g. 50 vol%, see Figure 8)

As the gold surface is activated by oxygen the amount of residual Ag – which was as already shown to be a key element for supplying activated oxygen in the case of CO oxidation - should have an impact on the activity and selectivity of the catalyst. To shed a light on this effect, samples containing different amounts of residual Ag were prepared by varying the preparation route. By reducing the time for leaching the Ag out of the starting alloy the amount of residual silver can be increased while the porous morphology of the material is preserved (*see experimental)*. By this method samples containing elevated amounts of Ag (2.5 at% and 10 at%) could be prepared and investigated for selective oxidation of methanol. As expected from UHV experiments, the selectivity drops with increasing amount of Ag and active oxygen, respectively. When using samples containing slightly elevated amounts of residual Ag (2.5 at%) the selectivity is at about 95 % close to 20 °C and decreases to about 70 % at 80 °C (see Figure 9). This characteristic resembles that of samples containing low fractions of Ag (~ 0.5 at%) in the case of high oxygen partial pressures (50 vol% cp to 1 vol%). This finding strongly suggests that the amount of Ag regulates the supply of activated oxygen on the surface, eventually leading to increased total oxidation and less selectivity. For samples containing about 10 at% residual Ag no activity towards the formation of methyl formate was observed at all. Only total oxidation (CO_2) was detected.

4 Actuation by nanoporous gold

(Relevant papers: III & IV)

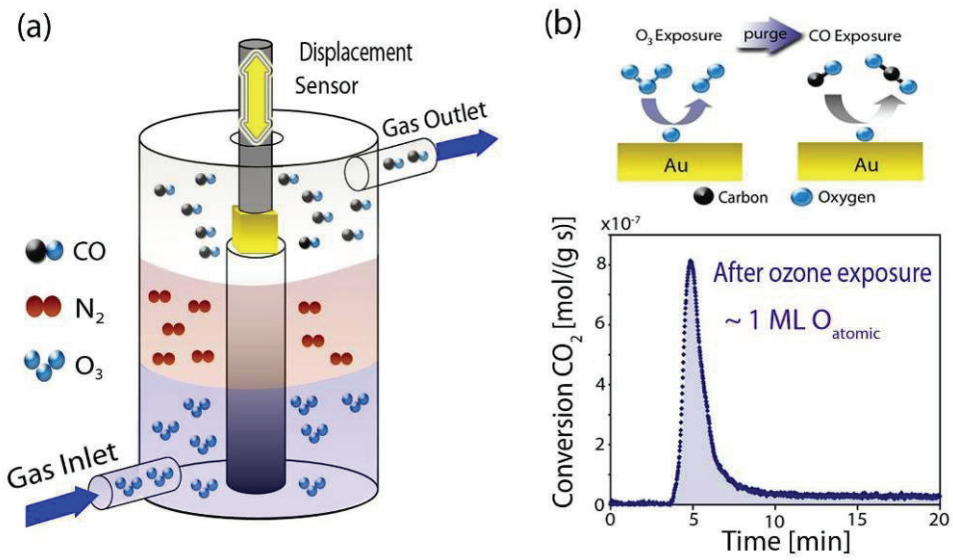

Figure 10: Surface chemistry induced actuation of np-Au. (a) The strain of a cubic sample of np-Au was measured as a function of the surrounding gases. (b) The exposure of ozone leads to coverage of the surface by atomic oxygen which can be removed by CO. A titration experiment of atomic oxygen with CO was carried out using the continuous flow reactor described in chapter 8.2. The amount of oxygen which is detected by this method corresponds to roughly one monolayer of atomic oxygen.

In the last chapters we discussed the catalysis by np-Au, this is the impact of the surface of np-Au on the surrounding gases. In the following two chapters we will discuss how the surrounding gases and their interaction with the surface of np-Au may have an impact on the material properties of np-Au itself. As described in chapter 2.2, the surface of a bulk material is subject to stress, the so called surface stress. The origin of this phenomenon can be understood on the basis of low coordination of surface atoms and the charge redistribution from unsaturated valences into in-plane bonds. Ibach and co-workers showed that the adsorption of molecules alter the surface stress of metals such as gold.(*36*) Accordingly, the surface stress of np-Au should be influenced by adsorption of molecules in a similar way than in an electrochemical environment, where the surface charge and surface coverage of a nanoporous metal can be changed by applying a potential. The change in surface charge inflicts a change in surface stress. Due to the exceptional high surface to volume ratio of nanoporous materials, this can lead to macroscopically detectable strain amplitudes, as for example, shown for electrodes of np-Au and np-Pt exhibiting strain amplitudes close or even equal to that of piezo ceramics.(*5, 33, 40*)

The same concept – circumventing previous production of electricity - can be applied as well using the adsorption of gases to influence the surface stress in np-Au. Here, oxygen is of high interest as the adsorption of atomic oxygen is known to lift the surface reconstruction.(*38, 102*) In contrast to molecular oxygen which does not dissociate on a pure gold surface, ozone (O_3) can be used to readily create surface bonded atomic oxygen.(*103*)

The surface bonded atomic oxygen is known to strongly react with CO (*67*) so that it can be removed easily (Figure 10(b)). Accordingly, we used the reaction O_3 + Au → O_2 + Au-O and CO + Au-O → CO_2 + Au to address the surface stress in np-Au in a setup schematically shown in Figure 10. A cubic sample of np-Au was placed in a cell to control the ambient atmosphere. The gases CO and O_3 were successfully fed into this cell; to prevent direct reaction the cell was always purged with N_2 in between cycles. The uniaxial strain was measured with a quartz rod contacting the outer surface of the cube of np-Au. The displacement of the quartz rod could be precisely measured.

For exposure of O_3 the sample shrank, this could be almost completely reversed by removal of oxygen with CO (Figure 11). Depending on the exposure time, the amplitude of strain amounts up to ~ 0.5 %. This corresponds to strain amplitudes of commercial piezo materials. The reversible part of the strain amplitude was nearly 100 percent. Freshly prepared samples however showed smaller reversibility which increased with lifetime. Secondly, the reversible part decreased when the total stroke increased. This indicates to a minor extend plastic deformation and to a major extent stress-driven creep which is more consistent with the slow kinetics.

It was found however that the preparation of samples is crucial for the effect of the surface chemistry on the surface stress and the sign of the strain. For example, when dealloying conditions are altered (e.g. dealloying at a different potential) the response of the np-Au material can be changed, as for example no shrinkage but expansion in case of ozone exposure can be observed. In an electrochemical environment Weismüller et al. showed that the pre-treatment of np-Au samples determined the sign of strain.(*104*) Under which conditions the sign of strain is reversed for adsorbate induced change of surface stress, however, remains a matter of future work.

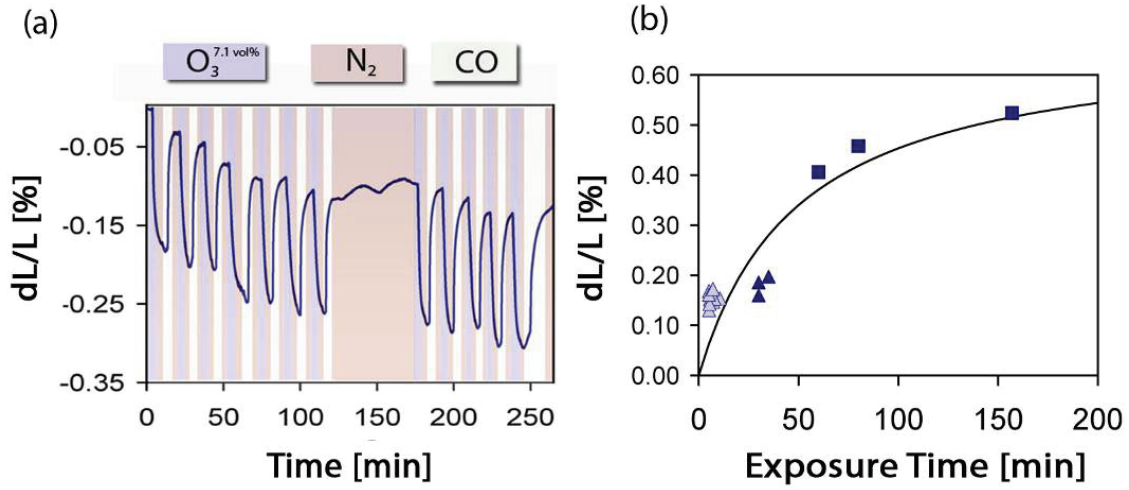

Figure 11: (a) Cycles of ozone and CO exposure lead to a reversible strain. Under an ozone containing atmosphere the sample shrinks, which can be reversed by removal of oxygen by reaction with CO. (b) The stroke amplitude (reversible part) increases with exposure time of O_3.

5 Tailoring structures of nanoporous gold

(Relevant papers: IV & V)

New material properties arise from reducing the length scale. Nevertheless, it is not only important to reduce the length scale but to tune and adjust the length scale for a specific application. In case of np-Au this means that the pore volume and size of ligaments have to be adjusted. As for example the catalytic activity of np-Au is a merit of the high fraction of low coordinated surface atoms, this number strongly depends on the diameter of the particular ligament (see Figure 3 on page 14). (*43, 45, 105*) Small ligaments therefore are beneficial for the catalytic activity; the mass transport within the pores of the material though is hampered when the pore volume is too small. This is a challenge which renders a bimodal pore structure very attractive. Secondly, applications in optics, e.g. surface enhanced Raman spectroscopy (SERS), are strongly dependant on the size of the ligaments and pores.(*106*) SERS enhancement factors were found to be maximal when the pores of np-Au were close to 250 nm.(*107*) Furthermore, the mechanical properties of np-Au are strongly dependant on size of the ligaments.(*108-109*) These examples exemplify that there is a need to tune and control the structural size of np-Au.

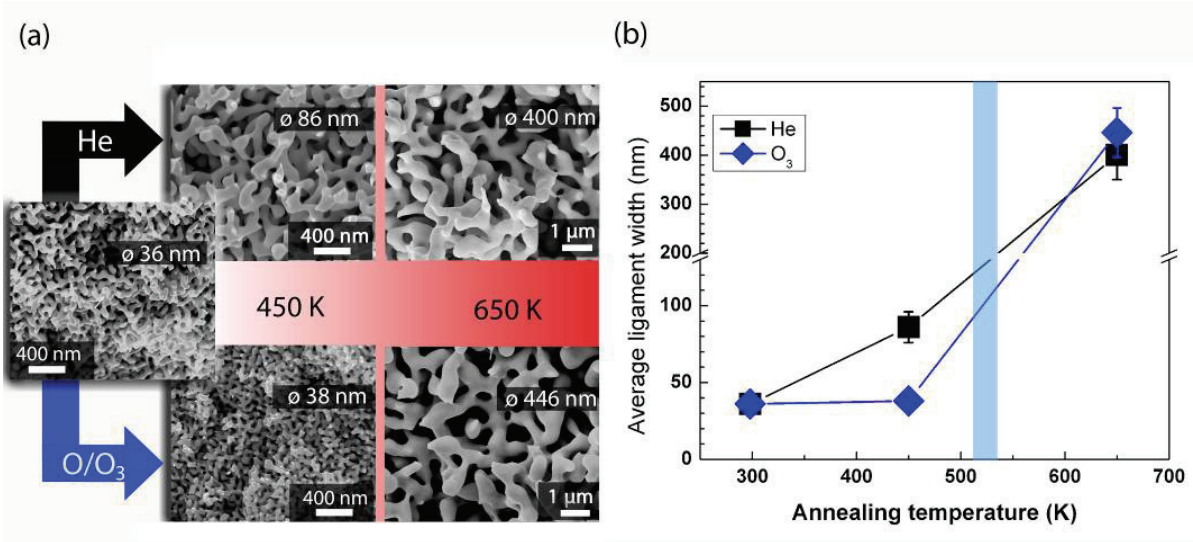

Figure 12: Tuning structure of np-Au. (a) Compilation of SEM images of np-Au after 3 hours of annealing under an inert gas atmosphere (He) and an ozone containing atmosphere (~ 6.5 vol% O_3 in O_2). (b) The evolution of the average ligament diameter as a function of the annealing temperature. Below the desorption temperature of atomic oxygen (indicated by blue column) the structure of np-Au is stabilized in an ozone containing atmosphere; almost no growth of ligaments is observable.

Coarsening in porous systems is typically ascribed to surface diffusion.(*110-111*) In case of metals this effect is at room temperature very slow (< 10^{-20} cm^2/s) but increases fast with temperature. Owing to this fact, the structure of np-Au is stable at room temperature, but starts coarsening when annealed at higher temperatures.(*107-108*) Already at temperatures of around 150 °C coarsening of the structures initiates and can be used to increase the

ligament and pore size.(*109*) However, two central challenges for designing structures in np-Au remain unattained, the stabilization i.e. conservation of the ligament size at elevated temperatures and the introduction of gradients. Both issues can be solved by means of adsorbate controlled surface diffusion of gold atoms.

The effect of surfactants on the stability of ligaments during annealing of np-Au was investigated. Samples of np-Au were annealed in an ozone containing atmosphere and, for comparison, in an inert gas atmosphere (He). When using ozone which readily decomposes on Au surfaces, the surface can be terminated by atomic oxygen.(*103*) Samples were treated for 3 hours in a tube furnace under continuous flow condition at 450 K, thus below the desorption temperature of atomic oxygen on gold, and above at 650 K, respectively. For characterization the samples were broken into two pieces and the particular size of ligaments along this cross section was investigated by SEM. The results for the ligaments close to the outer surface (~ 10 µm) are shown in Figure 12. At 450 K, i.e. below the desorption temperature of atomic oxygen, the structures of np-Au are stabilized as compared to samples annealed under He atmosphere. This is in line with scanning tunnelling microscopy studies in UHV environment which show that oxygen terminated structures – quite similar to those of np-Au - are considerably more persistent to coarsening.(*37*) Hardly any difference in size is detectable even after 6 hrs of treatment. On the contrary, at 650 K and thus above the desorption temperature of atomic oxygen the coarsening proceeds apparently un-effected from surrounding ozone. The size of the ligaments annealed under ozone atmosphere essentially equals that of ligaments annealed under He atmosphere.

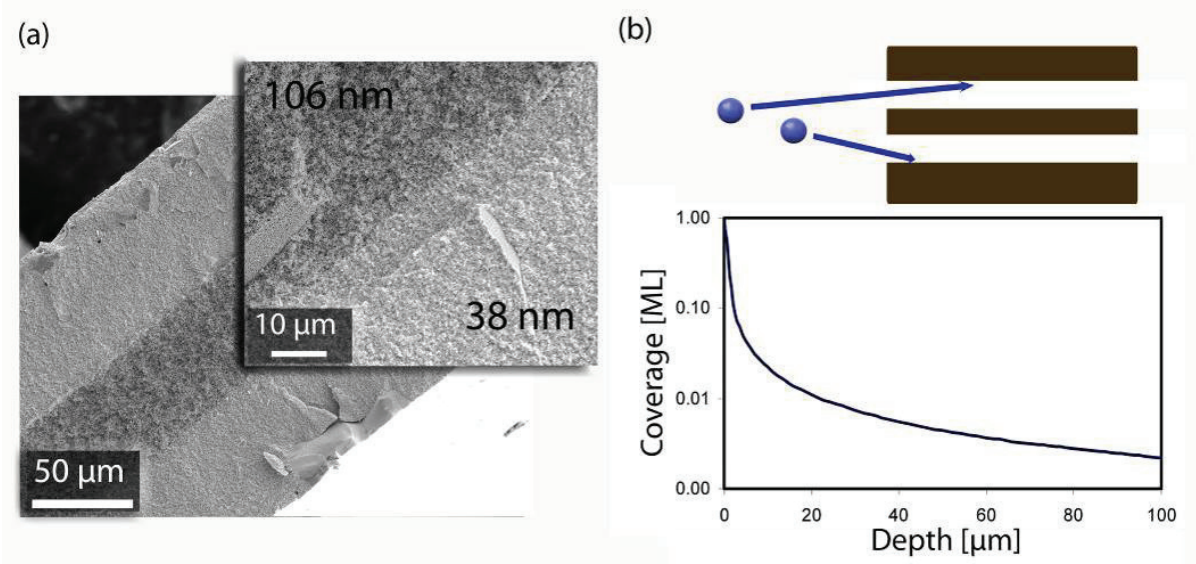

Figure 13: Gradients in ligament size can be induced using mass transport phenomena. A disk of np-Au was annealed for 3 hours at 450 K under an ozone containing atmosphere. (a) While the outer areas of the np-Au disk are stabilized by adsorbed oxygen ligaments in the inner section of the disk grew by about 300 %. (b) The effect of mass transport regulated growth of ligaments can be reproduced on the basis of a simple model where the adsorbate is supplied by the gas phase.

Using the stabilizing effect of ozone at lower temperatures, gradients of the ligament and pore size along the cross section of np-Au disks can be induced (see Figure 13). The coverage of the surface with atomic oxygen depends on the sticking time i.e. desorption energy and the supply from the gas phase (impingement rate and sticking probability). It is apparent, however, that the actual impingement rate is a function of the distance from the outer surface.(*112*) By assuming straight capillaries and based on thermochemistry data (*113*), this effect can be assessed as can be seen in Figure 13 (b). The inner surface of the material is not evenly covered with atomic oxygen; in fact the coverage exponentially decreases with the distance from the outer surface. Ligaments in the inner sections of the np-Au disk are thus not stabilized anymore and coarsening proceeds unhindered. In this way gradients in ligament and pore size can be introduced within the material.

Interestingly, the storage of samples had a decisive impact on the coarsening of the ligaments close to the outer surface. For samples stored in membrane boxes for a longer period of time (several days) gradients within the cross section of np-Au disks were observed after annealing at 650 K. After 3 hrs annealing at 650 K the average ligament diameter close to the outer surface (~ 10 μm) was only 200 nm as compared to 400 to 450 nm in the inner section. Presumably, contaminants originating from the contact of the outer surface with the plastic of the membrane box led to the observed effect. In order to further elucidate this effect samples were pre-treated with an ozone containing atmosphere. This treatment is supposed to create active (atomic) oxygen on the surface and thus guarantee good cleaning by oxidation of carbon containing contaminants. Indeed, no gradient along the cross section was observed anymore. This implies that carbon containing contaminants e.g. hydrocarbons initially present on the outer surface can have a stabilizing effect on the ligaments and prevent coarsening.

These examples, the stabilization of ligaments by ozone at lower temperatures or surfactants like hydrocarbons at higher temperatures, reflect the importance of adsorbates on the stability of the nanostructure of np-Au. It is also a descriptive example of the impact of adsorbates on the mobility of surface atoms, and thus coarsening.

6 Outlook: Surface engineering and doping of np-Au

(relevant papers IV & VI)

The use of the inherent material properties of np-Au is certainly limited. As already shown for the activation of molecular oxygen in the chapters 3.1 and 3.2, the presence of residual Ag within the material can play a beneficial role and extends the limitations posed by the intrinsic surface chemistry of gold. It is, however, tempting to further expand the possible applications of np-Au by doping or depositing other materials, such as metals (Pt, Pd) and semiconductors (CeO_2, TiO_2), in the porous structure. For example the addition of Pt particles on np-Au working as a substrate has been shown to be promising for applications in fuel cells. (*54, 114*) Furthermore, material systems comprised of TiO_2 layers or nanoparticles on Au substrates attracted considerable attention, not only because such systems constitute inverse systems to oxide supported Au nanoparticles (*115-116*) but also because of their altered electronic properties (*117-118*) which hold out interesting applications in photo catalysis (*51*), photovoltaic devices (*119*) and water splitting reactions (*120*). Recently, Ding et al. showed that by implementing TiO_2 particles in np-Au films the electro-catalytic activity of gold for methanol oxidation can indeed be sensitised to UV irradiation.(*51*)

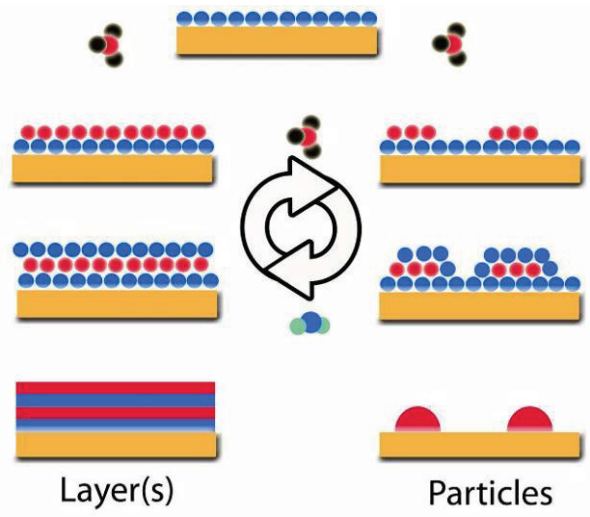

Figure 14: Atomic layer deposition (ALD) is based on the self limiting reaction of a precursor on the material surface. Within the first half-cycle of ALD the precursor is dosed onto the surface, the deposition though is restricted to the reaction with active surface sites. After depletion of active sites no further deposition occurs. In a second half cycle, the active sites on the surface have to be regenerated. The deposition within one complete deposition cycle is limited to 1 monolayer. Depending on the growth mechanism layers as well as particles can be grown.

However, the well-directed deposition of material within np-Au poses a challenge due to its mesoporous structure with pores between 20 and 50 nm in size. In case of thin films (~ 100 nm) of np-Au the mass transport limitation plays only a minor role and experimentally facile “bench-top” methods can be used. (*51, 114*) Applications such as electrodes in fuel cells or catalytic membranes though typically require the use of freestanding and thus much thicker materials in the range of several microns ore even millimetres. The ultra high aspect ratio of those materials in the order of more than several thousands calls for more

sophisticated methods to guarantee a conformal and precise deposition of the possibly very expensive dopant/deposit. In this context the atomic layer deposition (ALD) showed great potential for depositing nanoparticles in ultra high aspect ratio materials.(*121-124*) For example, by using ALD, high aspect ratio materials could be functionalized with beforehand unrealised small amounts of Pt creating a highly active and effective catalyst (see Figure 15).(*125*) In order to further launch applications of np-Au it will be of great importance to draw on the potential of sophisticated doping techniques like the atomic layer deposition.

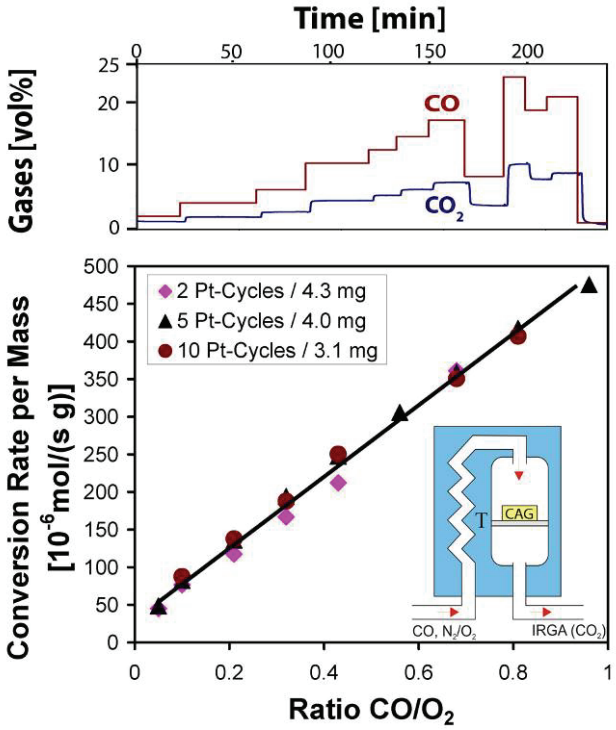

Figure 15: Catalytic oxidation of CO using a Pt functionalized carbon aerogel. Due to high aspect ratio of the aerogel the ALD method proved to be particularly suitable to deposit unprecedented small amounts of Pt. Upper section: The time series of CO at the inlet of the reactor (see inset) and the corresponding concentration of CO_2 detected at the outlet. Lower section: The catalytic activity increases linearly with the supply of CO, this indicates that all CO supplied is converted to CO_2. The maximal i.e. total conversion is already achieved by the smallest possible amount of Pt using 2 cycles of ALD. This result underlines the importance of tailoring the deposition of precious Pt as a key element for high economic viability.

7 Summary

The fabrication and applications of np-Au were investigated with the emphasis on catalysis, actuation, and structural control during annealing. The observed characteristics were interpreted and discussed with the perspective on surface related phenomena.

First, the catalytic activity of np-Au for gas phase reactions was investigated using the oxidation of CO. After activation of samples the kinetics of the reaction was determined. To further shed light on the catalytic activity of np-Au with respect to residual Ag and the activation of molecular oxygen, samples containing different amounts of Ag were investigated. In general, the activity increased with increasing amount of Ag. These results strongly suggest that Ag participates in the catalytic cycle. A first interpretation of the role of Ag as the crucial element for the activation of molecular oxygen was proposed based on kinetics and model experiments under UHV conditions.

To further highlight the catalytic characteristics of np-Au the gas phase oxidative coupling of methanol was investigated. The formation of methyl formate could be detected already at 20 °C and further increased for higher temperatures. Notably, the formation of an ester (and not of the aldehyde or acid) is fully in line with what has been observed for pure gold surfaces so that the general catalytic behaviour is nearly completely understood and anticipated on the molecular level based on UHV model experiments. Solely the activation of oxygen on np-Au is not explainable on the basis of single crystal experiments so far. In this work, it was found that activity and selectivity are strongly dependant on the fraction of Ag within the material. In the case of increasing content, the partial oxidation considerably decreased and total oxidation was increasingly favoured. Finally, at 11 at% Ag the only observed product was CO_2. This finding can be explained by an increased supply of activated oxygen and suggest that Ag regulates the availability of reactive oxygen on the surface.

In addition, the impact of surface chemistry on the material properties was investigated with respect to actuation and structural control during annealing. The surface of np-Au was reversibly covered with atomic oxygen taking advantage of the decomposition of ozone. In case of actuation experiments, the oxygen coverage was escorted by a macroscopically detectable stroke of the sample which was reversibly lifted by its removal with CO. This experiment exemplifies the importance of surface chemistry induced stress in case of high surface to volume ratio materials. For structural control during annealing of np-Au samples, the impact of coordination (i.e. bonding to oxygen) on the surface diffusion of gold atoms was used to stabilize the structure or even induce gradients in ligament and pore size.

8 Experimental

8.1 Synthesis of master alloy and Preparation of np-Au

The Au and Ag metals were supplied by the department of energy (DOE). The desired composition of the alloy was 70 at% Ag and 30 at% Au, corresponding to a mass ratio of 56.11 wt% Ag and 43.89 wt% Au. Giving an example, 29.7953 g of alloy were produced by mixing 18.3417 g Ag and 13.0760 g Au. Both metals were brought into the form of chippings in order to guarantee good mixing during melting. The chippings were carefully cleaned by sonication for 30 minutes in isopropanol. A graphite crucible filled with the metal chipping was brought into a preheated muffle oven. The oven was then heated to 1100 °C. After 15 minutes the crucible was carefully rotated to guarantee good mixing of both metals. After a total of 40 minutes the cast was poured into a graphite form, rapidly cooling and forming bars of the desired alloy. After weighing of the bar, the alloy was annealed under an Ar atmosphere for 140 hrs at 875 °C. Repeatedly, the alloy was weighed in order to check any loss of material. Subsequently, the bar was cut with a diamond saw into slices of about 5 mm thickness. These slices were rolled into work pieces of about 200 to 300 µm thickness. The pieces were cut into round disks by punching (diameters of 4.8 mm and 6.7 mm, respectively). The alloy disks were again annealed at 800 °C for 4 hours so that residual stress originated from rolling and cutting was released. All samples were cleaned by sonication in isopropanol for about 30 minutes. Finally, the composition of the alloy disks was controlled by energy dispersive X-ray spectroscopy (EDX). The deviation from the set values (Ag 70 at% and Au 30 at%) was less than 1 at% and thus very close to the accuracy limit of EDX.

The preparation of np-Au, that means the dissolution of Ag from the Ag-Au alloy, was done either by “free corrosion” or “potentiostatic corrosion”. For free corrosion no external potential was applied, the open-circuit potential of the alloy caused the dissolution of Ag. The alloy disks were immersed in concentrated nitric acid (65 wt%, Fluka Chemical Corp.) on a glass fritt. After 48 hrs the acid was replaced by deionised water, which was replaced at least three times after 1 hour each. For potentiostatic corrosion the sample was place into a basket formed by a gold wire. Using a typical three electrode setup, the sample was immersed in a 5 M solution of nitric acid and dealloyed at a potential of 60 mV (HNO_3 from Fluka, dissolved in ultra pure water, > 18 MΩ) (working electrode: gold wire containing the alloy disk, counter- and reference electrode: Pt) (Figure 17). Generally, the residual Ag content was checked by weight analysis. In several cases samples were also characterized by X-ray photoemission spectroscopy (XPS), and energy dispersive X-ray spectroscopy (EDX) (see Figure *16*). Although these spectroscopic techniques are non-destructive the detection limit of EDX of about 1 at% for Ag renders – if necessary - atomic absorption spectroscopy (AAS) useful to precisely quantify such low Ag contents.

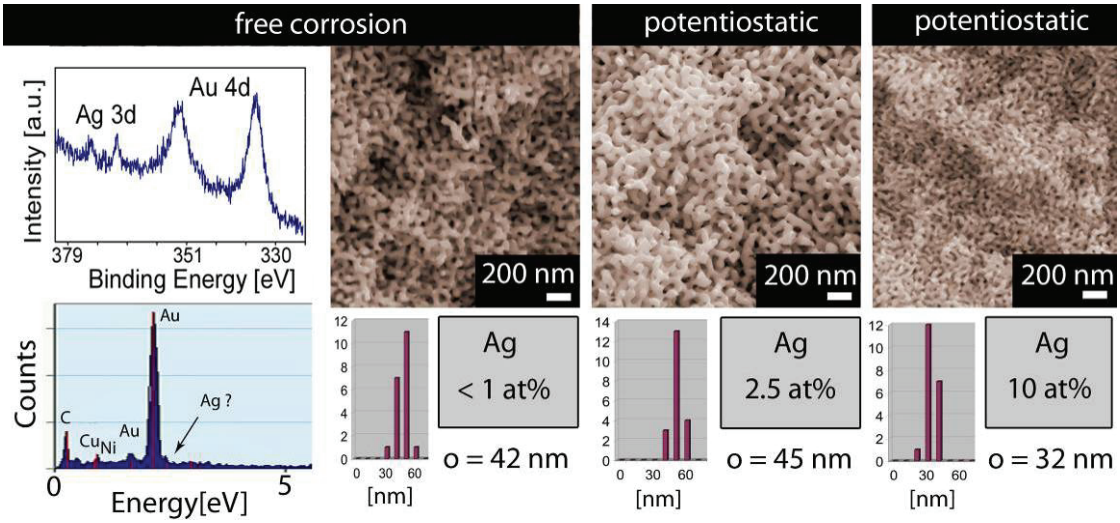

Figure 16: Analysis of differently prepared np-Au. Samples as either prepared by free or potentiostatic corrosion. On the very left an XP spectrum showing the Ag 3d and Au 4d region, verifying that Ag is indeed enriched at the surface (about 8 at%) while the EDX analysis shows no clear signal from the residual Ag. This is a consequence of the detection limit of EDX of about 1 at%. For characterization of morphology the samples were broken and the middle of the particular cross section was investigated by SEM. The average ligament diameter and the corresponding histogram are displayed. On the very right, a characterization of a sample is shown which was dealloyed for 32 hours and thus containing a higher fraction of residual silver.

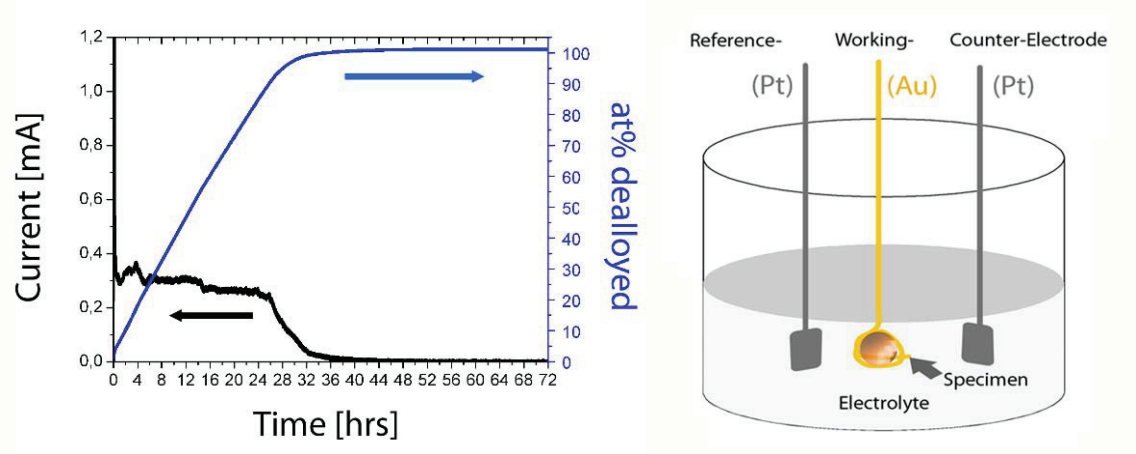

Figure 17: Potentiostatic corrosion of a $Ag_{70}Au_{30}$ alloy disk in 5 M nitric acid. The sample was placed into a basked formed by a gold wire. On the right: Using a typical three electrode setup the sample was held at constant potential (60 mV vs. Pt). On the left: Based on the current between the sample (working electrode) and the counter electrode the amount of Ag dissolved can be calculated (assuming every electron originated from the dissolution of one Ag metal atom). At about 30 hours the current steeply decreases. This corresponds to a rapid drop in the corrosion rate of Ag.

8.2 Catalytic investigation

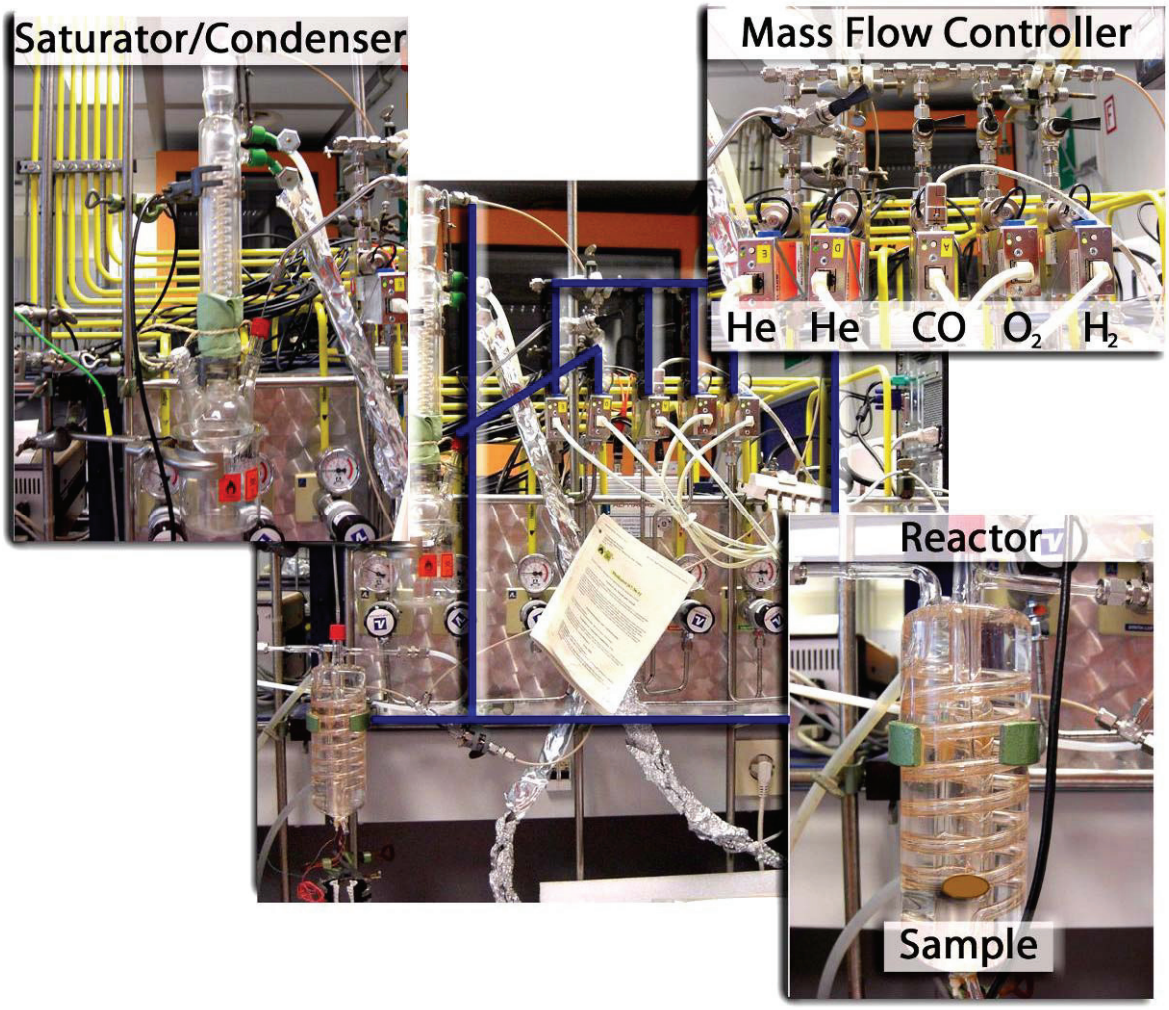

Figure 18: Experimental setup for measuring the catalytic performance of np-Au. Flow and composition of gases were precisely controlled via mass flow controllers (upper right). The stream of gases (highlighted by blue lines) was guided towards the reactor (enlarged on the lower right). For experiments using e.g. methanol an additional He stream was guided through a system of saturator and condenser to precisely adjust the content of the particular liquid in the gas phase.

The catalytic experiments were performed in a continuous flow reactor. A schematic of the setup is shown in Figure 19. An overview of the experimental setup using photographs is depicted in Figure 18. The double walled reactor was completely made of glass, and its inner diameter was around 20 mm with a total volume of 26 ml. The inlet tubing was guided through a circled pipe through the outer compartment of the reactor which was heated and cooled, respectively, by a thermostat. This procedure guaranteed a maximal control over the temperature of the gases. The samples were placed at the lower end of the reactor on a gold plate with an opening in the center. The mass of the gold plate was 2.2 g, thus around 100 times that of the catalyst disk. In this way, a large part of the heat originating from catalytic

conversion was rapidly dissipated. Isothermal conditions were intended. The inlet gas was directed through the opening in the middle of the gold plate and thus directly guided towards the sample; in consequence it was avoided that large parts of the feed bypassed the sample. The feed gases were He (*Linde AG*, 5.0), O_2 (*Linde AG*, 4.5), CO (*Linde AG*, 4.7), and H_2 (*Linde AG*, 5.0). The total flow was always set to 50 sccm. The composition was precisely controlled via mass flow controllers (Maettig Bronkhorst, Netherlands).

For experiments using compounds which are liquids under ambient conditions the particular concentration in the gas phase was controlled by its vapour pressure. For this purpose a stream of He was guided through a saturator coupled with a condenser (see Figure 18). In the following the procedure using methanol is described. In principle the same procedure was used for experiments using other liquids such as water or acetaldehyde. First, the gas stream was saturated with methanol at room temperature (around 20 °C), subsequently the amount of methanol in the gas phase was adjusted by directing the stream of saturated gas trough a cooling pipe. Due to lower vapour pressure at lower temperatures, excess methanol condensed. Following this procedure, stable and precise methanol concentrations were achieved. The particular vapour pressure of methanol at different temperatures was calculated using the KDB database (Korea Thermophysical Database, see Figure 20). Prior to measurements, the methanol was dried in order to remove any water. Therefore, methanol (NORMAPUR, 99.8 %, VWR) was mixed with magnesium chipping (8 g per 500 ml) and boiled under reflux for 3 hours. The dried methanol was obtained by distillation under dry gas atmosphere. The stream of gases at the exit of the reactor was monitored online by IR-Gas-Analyzers (URAS 3G, Hartmann und Braun, highly sensitive for CO and CO_2). Additionally, the composition of the gas stream was investigated by GC-MS. The content of a sample pipe (100 µl) was injected into a gas chromatograph (Fison 8000 series, Column FS-innopeg-1000) coupled with a mass spectrometer (TRIO 1000).

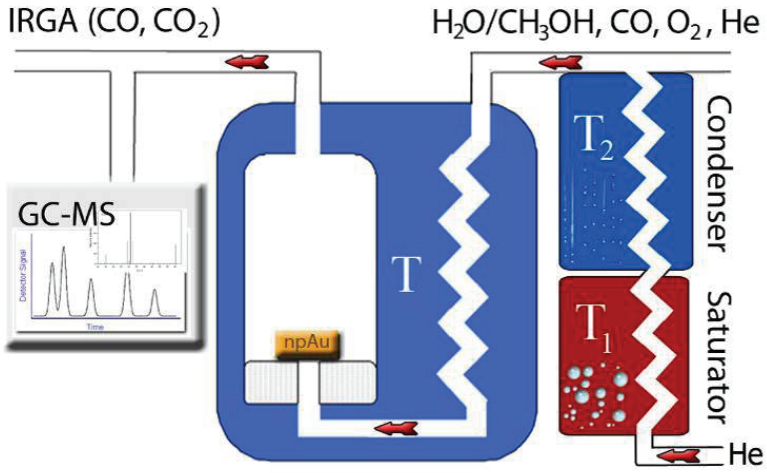

Figure 19: Schematic of the experimental setup for measuring the catalytic conversion of CO and methanol, respectively. The content of methanol or water in the feed gases were adjusted by their vapour pressure. A stream of carrier gas (He) was saturated, in a second step the precise partial pressure of the particular component was controlled by condensation. The disk of np-Au was placed on a gold plate at the bottom of the reactor. The stream of reactant gases is guided through an opening of the gold plate onto the disk. At the reactor outlet the composition of the gas stream was investigated by IR and GC-MS.

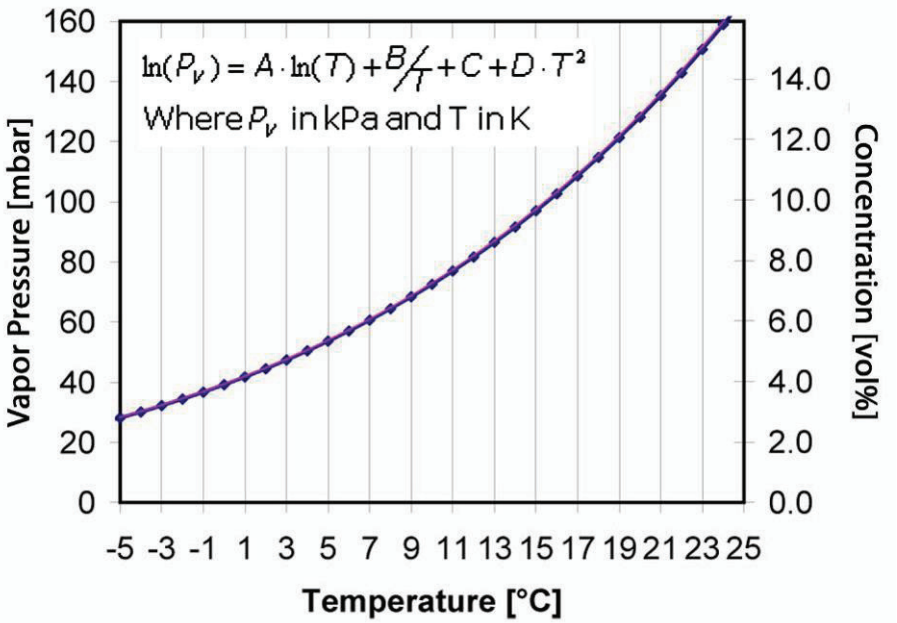

Figure 20: Vapor pressure of methanol and the corresponding concentration (partial pressure) within the gas phase assuming 1 bar total pressure. The pressure was calculated based on the KDB database (coefficients A =-9.372816, B = $-7\cdot10^3$, C = 79.09415, D =$8\cdot10^{-6}$)

8.3 Measuring actuation of np-Au

The experiments regarding the measurement of surface chemistry induced actuation of nanoporous gold were performed at the Institut für Nanotechnology (INT) at the Forschungszentrum Karlsruhe. Pictures of the experimental setup are shown in Figure 21. The np-Au samples were supplied by INT. The master alloy of the particular samples was $Ag_{65}Au_{35}$ which was dealloyed at 55 °C in $HClO_4$ at a potential of 650 mV vs. Ag/AgCl (dealloying was stopped when the anodic current was negligible small). The dimensions of the cubic sample were 1x1x1 mm^3. For measurement the sample was placed in a sample compartment to control the composition of the surrounding gases. The stroke of the sample was detected by a quartz rod which was in contact with the surface of the np-Au cube.

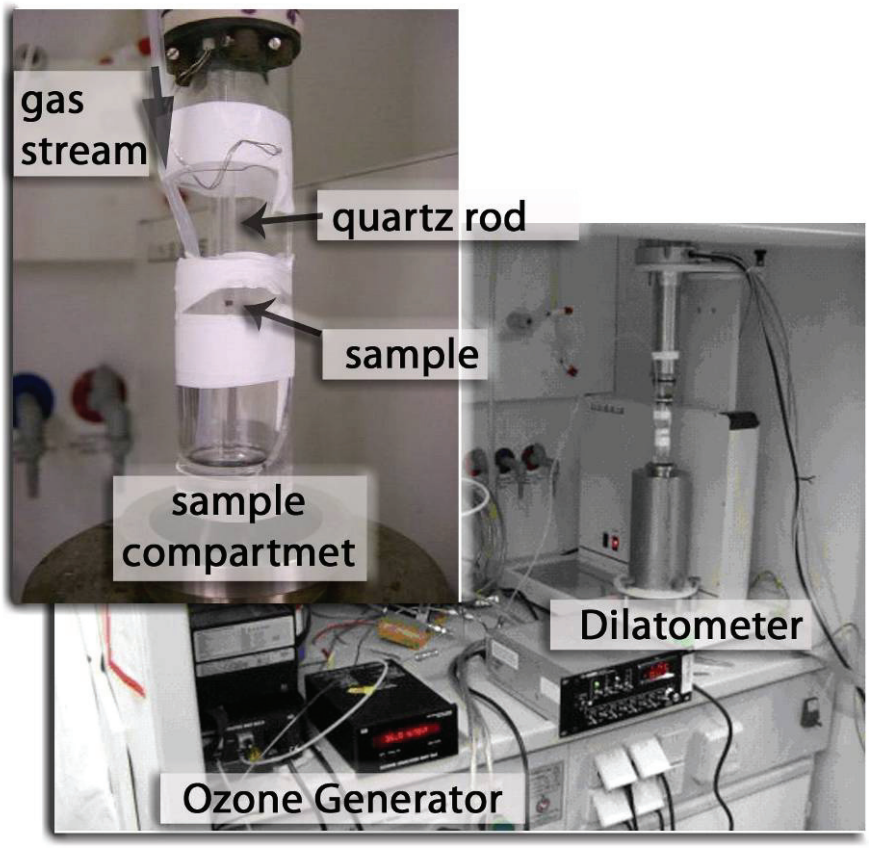

Figure 21: Photographs of the experimental setup for measuring surface chemistry driven actuation of np-Au

8.4 Annealing Experiments

The annealing experiments were conducted using an experimental setup shown in Figure 22. At first a disk of np-Au was broken into several pieces (e.g. 4) so that in any case at least one piece remained untreated as reference. For annealing the particular sample piece was placed within a tube furnace made of quartz glass. To prevent direct contact with the glass tube the sample was embedded in quartz wool, a homogeneous distribution of heat through the gas phase was intended. In order to precisely measure the temperature within the tube furnace a thermocouple (Cr/NiCr) was placed close to the sample (about 1 cm distance). The stream velocity of gas (He 5.0 Linde AG and O_2 4.5 Linde AG) was adjusted by rotameters (variable area flow meters) to 50 ml/min. Before heating up the furnace the entire compartment was purged with the particular gas for one hour. For experiments using an ozone containing atmosphere the stream of O_2 was guided through an ozone generator (BMT Messtechnik, BMT 802 N), the actual content of ozone was controlled by an ozone analyzer (BMT Messtechnik, BMT 964).

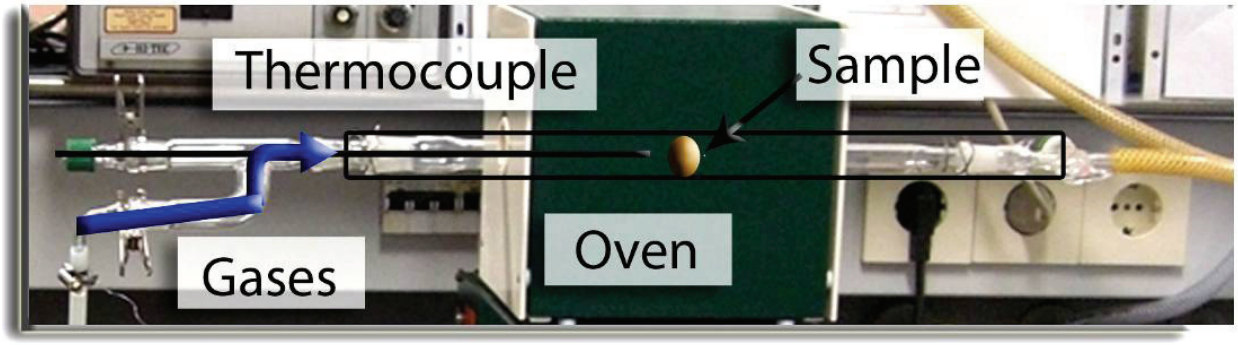

Figure 22: Experimental setup for annealing of np-Au under different atmospheres

9 References

1. H. Renner *et al.*, in *Ullmann's Encyclopedia of Industrial Chemistry*. (Wiley-VCH, Weinheim, 2000).
2. M. Haruta, T. Kobayashi, H. Sano, N. Yamada, *Chemistry Letters*, 405 (1987).
3. G. J. Hutchings, *J. Catal.* **96**, 292 (1985).
4. C. W. Corti, R. J. Holliday, D. T. Thompson, *Top. Catal.* **44**, 331 (Jun, 2007).
5. J. Biener *et al.*, *Materials* **2**, 2404 (2009).
6. J. Lee *et al.*, *Chem. Soc. Rev.* **38**, 1450 (2009).
7. J. Erlebacher, R. Seshadri, *MRS Bull.* **34**, 561 (Aug, 2009).
8. Z. H. Zhang *et al.*, *J. Phys. Chem. C* **113**, 12629 (Jul, 2009).
9. R. C. Newman, K. Sieradzki, *MRS Bull.* **24**, 12 (Jul, 1999).
10. R. C. Newman, S. G. Corcoran, J. Erlebacher, M. J. Aziz, K. Sieradzki, *MRS Bull.* **24**, 24 (Jul, 1999).
11. Y. Ding, Y. J. Kim, J. Erlebacher, *Adv. Mater.* **16**, 1897 (Nov, 2004).
12. A. J. Forty, *Nature* **282**, 597 (1979).
13. H. W. Pickering, *Corrosion Sci.* **23**, 1107 (1983).
14. H. W. Pickering, P. R. Swann, *Corrosion* **19**, 373t (1963, 1963).
15. A. J. Forty, P. Durkin, *Philosophical Magazine a-Physics of Condensed Matter Structure Defects and Mechanical Properties* **42**, 295 (1980).
16. Y. Ding, M. W. Chen, *MRS Bull.* **34**, 569 (Aug, 2009).
17. E. Seker, M. Reed, M. Begley, *Materials* **2**, 2188 (2009).
18. S. Kameoka, A. P. Tsai, *Catal. Lett.* **121**, 337 (Mar, 2008).
19. S. Kameoka, A. P. Tsai. (Elsevier Science Bv, Seoul, SOUTH KOREA, 2007), pp. 88-92.
20. X. G. Wang, Z. Qi, C. C. Zhao, W. M. Wang, Z. H. Zhang, *J. Phys. Chem. C* **113**, 13139 (Jul, 2009).
21. Z. Qi *et al.*, *J. Phys. Chem. C* **113**, 6694 (Apr, 2009).
22. A. Wittstock, V. Zielasek, J. Biener, C. M. Friend, M. Baumer, *Science* **327**, 319 (January 15, 2010, 2010).
23. G. Tammann, *Z. Anorg. Allg. Chem.* **107**, 1 (Jul, 1919).
24. G. Masing, *Naturwissenschaften* **11**, 413 (1923).
25. A. Dursun, D. B. Pugh, S. G. Corcoran, *J. Electrochem. Soc.* **152**, B65 (2005).
26. A. Dursun, D. V. Pugh, S. G. Corcoran, *Electrochemical and Solid State Letters* **6**, B32 (Aug, 2003).
27. A. Dursun, D. V. Pugh, S. G. Corcoran, *J. Electrochem. Soc.* **150**, B355 (Jul, 2003).
28. D. M. Artymowicz, J. Erlebacher, R. C. Newman, *Philos. Mag.* **89**, 1663 (2009).
29. J. Erlebacher, *J. Electrochem. Soc.* **151**, C614 (2004).
30. J. Erlebacher, M. J. Aziz, A. Karma, N. Dimitrov, K. Sieradzki, *Nature* **410**, 450 (Mar, 2001).
31. L. H. Qian, M. W. Chen, *Appl. Phys. Lett.* **91**, (Aug, 2007).
32. J. Biener *et al.*, *Nature Materials* **8**, 47 (Jan, 2009).
33. J. Weissmuller *et al.*, *Science* **300**, 312 (Apr, 2003).
34. W. Haiss, *Reports on Progress in Physics* **64**, 591 (May, 2001).
35. H. Ibach, *Surf. Sci. Rep.* **29**, 195 (1997).
36. C. E. Bach, M. Giesen, H. Ibach, T. L. Einstein, *Phys. Rev. Lett.* **78**, 4225 (Jun, 1997).
37. J. Biener *et al.*, *ChemPhysChem* **7**, 1906 (Sep, 2006).
38. B. K. Min, A. R. Alemozafar, M. M. Biener, J. Biener, C. M. Friend, *Top. Catal.* **36**, 77 (Aug, 2005).
39. H. J. Jin *et al.*, *Acta Mater.* **57**, 2665 (May, 2009).

40. D. Kramer, R. N. Viswanath, J. Weissmuller, *Nano Lett.* **4**, 793 (May, 2004).
41. W. L. Yim *et al.*, *J. Phys. Chem. C* **111**, 445 (Jan, 2007).
42. J. Greeley, J. K. Norskov, M. Mavrikakis, *Annual Review of Physical Chemistry* **53**, 319 (2002).
43. J. K. Norskov *et al.*, *Chem. Soc. Rev.* **37**, 2163 (Oct, 2008).
44. J. K. Norskov *et al.*, *J. Catal.* **209**, 275 (Jul, 2002).
45. H. Falsig *et al.*, *Angew. Chem.-Int. Edit.* **47**, 4835 (2008).
46. V. Zielasek *et al.*, *Angew. Chem.-Int. Edit.* **45**, 8241 (2006).
47. C. X. Xu *et al.*, *J. Am. Chem. Soc.* **129**, 42 (Jan, 2007).
48. G. C. Bond, D. T. Thompson, *Gold Bull.* **33**, 41 (2000).
49. G. C. Bond, D. T. Thompson, *Catalysis Reviews-Science and Engineering* **41**, 319 (1999).
50. H. M. Yin *et al.*, *J. Phys. Chem. C* **112**, 9673 (Jul, 2008).
51. C. C. Jia *et al.*, *J. Phys. Chem. C* **113**, 16138 (Sep, 2009).
52. J. T. Zhang, P. P. Liu, H. Y. Ma, Y. Ding, *J. Phys. Chem. C* **111**, 10382 (Jul, 2007).
53. Y. Ding, M. W. Chen, J. Erlebacher, *J. Am. Chem. Soc.* **126**, 6876 (Jun, 2004).
54. R. Zeis, T. Lei, K. Sieradzki, J. Snyder, J. Erlebacher, *J. Catal.* **253**, 132 (Jan, 2008).
55. C. L. Bracey, P. R. Ellis, G. J. Hutchings, *Chem. Soc. Rev.* **38**, 2231 (2009).
56. J. L. Gong, C. B. Mullins, *Accounts Chem. Res.* **42**, 1063 (Aug, 2009).
57. M. Bowker, *Chem. Soc. Rev.* **37**, 2204 (Oct, 2008).
58. N. Bion, F. Epron, M. Moreno, F. Marino, D. Duprez, *Top. Catal.* **51**, 76 (Dec, 2008).
59. A. Wittstock *et al.*, *The Journal of Physical Chemistry C* **113**, 5593 (2009).
60. W. J. T. John Meurig Thomas, *Principle and Practice of Heterogeneous Catalysis*. (Weinheim, New York, Basel, Cambridge, Tokyo, October 1996).
61. J. M. Gottfried, K. J. Schmidt, S. L. M. Schroeder, K. Christmann, *Surf. Sci.* **536**, 206 (Jun, 2003).
62. J. M. Gottfried, K. J. Schmidt, S. L. M. Schroeder, K. Christmann, *Surf. Sci.* **525**, 184 (Feb, 2003).
63. J. M. Gottfried, K. J. Schmidt, S. L. M. Schroeder, K. Christmann, *Surf. Sci.* **525**, 197 (Feb, 2003).
64. J. M. Gottfried, N. Elghobashi, S. L. M. Schroeder, K. Christmann, *Surf. Sci.* **523**, 89 (Jan, 2003).
65. J. M. Gottfried, K. Christmann. (Elsevier Science Bv, Prague, CZECH REPUBLIC, 2003), pp. 1112-1117.
66. J. M. Gottfried, K. J. Schmidt, S. L. M. Schroeder, K. Christmann, *Surf. Sci.* **511**, 65 (Jun, 2002).
67. B. K. Min, A. R. Alemozafar, D. Pinnaduwage, X. Deng, C. M. Friend, *J. Phys. Chem. B* **110**, 19833 (Oct, 2006).
68. S. Y. Quek, C. M. Friend, E. Kaxiras, *Surf. Sci.* **600**, 3388 (Sep, 2006).
69. J. Pawelacrew, R. J. Madix, J. Stohr, *Surf. Sci.* **339**, 23 (Sep, 1995).
70. M. A. Barteau, R. J. Madix, *J. Chem. Phys.* **74**, 4144 (1981).
71. M. A. Barteau, R. J. Madix, *Surf. Sci.* **97**, 101 (1980).
72. M. Bowker, M. A. Barteau, R. J. Madix, *Surf. Sci.* **92**, 528 (1980).
73. G. McElhiney, H. Papp, J. Pritchard, *Surf. Sci.* **54**, 617 (1976).
74. Y. Iizuka *et al.*, *J. Catal.* **262**, 280 (Mar, 2009).
75. Y. Iizuka *et al.*, *Catal. Lett.* **97**, 203 (Sep, 2004).
76. A. Q. Wang, Y. Hsieh, Y. F. Chen, C. Y. Mou, *J. Catal.* **237**, 197 (Jan, 2006).
77. A. Q. Wang, J. H. Liu, S. D. Lin, T. S. Lin, C. Y. Mou, *J. Catal.* **233**, 186 (Jul, 2005).
78. J. H. Liu, A. Q. Wang, Y. S. Chi, H. P. Lin, C. Y. Mou, *J. Phys. Chem. B* **109**, 40 (Jan, 2005).

79. D. I. Kondarides, X. E. Verykios, *J. Catal.* **158**, 363 (Feb, 1996).
80. R. G. Quiller *et al.*, *J. Chem. Phys.* **129**, 9 (Aug, 2008).
81. M. Date, M. Haruta, *J. Catal.* **201**, 221 (Jul, 2001).
82. L. M. Liu, B. McAllister, H. Q. Ye, P. Hu, *J. Am. Chem. Soc.* **128**, 4017 (Mar, 2006).
83. Z. L. Wu, S. H. Zhou, H. G. Zhu, S. Dai, S. H. Overbury, *J. Phys. Chem. C* **113**, 3726 (Mar, 2009).
84. H. Y. Su, M. M. Yang, X. H. Bao, W. X. Li, *J. Phys. Chem. C* **112**, 17303 (Nov, 2008).
85. N. Dimitratos, J. A. Lopez-Sanchez, G. J. Hutchings, *Top. Catal.* **52**, 258 (Apr, 2009).
86. M. Poliakoff, P. Licence, *Nature* **450**, 810 (Dec, 2007).
87. V. Gewin, *Nature* **440**, 378 (2006 Mar, 2006).
88. M. Toda *et al.*, *Nature* **438**, 178 (Nov, 2005).
89. D. Bradley, *Science* **300**, 2022 (Jun, 2003).
90. C. Marsden *et al.*, *Green Chem.* **10**, 168 (2008).
91. E. Taarning, A. T. Madsen, J. M. Marchetti, K. Egeblad, C. H. Christensen, *Green Chem.* **10**, 408 (2008).
92. B. K. Min, C. M. Friend, *Chem. Rev.* **107**, 2709 (Jun, 2007).
93. T. Ishida, M. Haruta, *Angew. Chem.-Int. Edit.* **46**, 7154 (2007).
94. M. D. Hughes *et al.*, *Nature* **437**, 1132 (Oct, 2005).
95. M. Haruta, *Gold Bull.* **34**, 40 (2001).
96. X. Y. Liu, R. J. Madix, C. M. Friend, *Chem. Soc. Rev.* **37**, 2243 (Oct, 2008).
97. E. Fiedler, G. Grossmann, D. B. Kersebohm, G. Weiss, C. Witte, in *Ullmann's Encyclopedia of Industrial Chemistry*. (Wiley-VCH Verlag GmbH & Co. KGaA, Weinheim, 2000).
98. G. Reuss, W. Disteldorf, A. O. Gamer, A. Hilt, in *Ullmann's Encyclopedia of Industrial Chemistry*. (Wiley-VCH Verlag GmbH & Co. KGaA, Weinheim, 2000).
99. W. Reutemann, H. Kieczka, in *Ullmann's Encyclopedia of Industrial Chemistry*. (Wiley-VCH Verlag GmbH & Co. KGaA, Weinheim, 2000).
100. B. J. Xu, X. Y. Liu, J. Haubrich, R. J. Madix, C. M. Friend, *Angew. Chem.-Int. Edit.* **48**, 4206 (2009).
101. R. J. Madix, C. M. Friend, X. Y. Liu, *J. Catal.* **258**, 410 (Sep, 2008).
102. B. K. Min, X. Deng, D. Pinnaduwage, R. Schalek, C. M. Friend, *Physical Review B* **72**, (Sep, 2005).
103. N. Saliba, D. H. Parker, B. E. Koel, *Surf. Sci.* **410**, 270 (Aug, 1998).
104. H. J. Jin, S. Parida, D. Kramer, J. Weissmuller, *Surf. Sci.* **602**, 3588 (Dec, 2008).
105. J. K. Norskov, T. Bligaard, J. Rossmeisl, C. H. Christensen, *Nat. Chem.* **1**, 37 (Apr, 2009).
106. J. Biener *et al.*, *Adv. Mater.* **20**, 1211 (Mar, 2008).
107. S. O. Kucheyev *et al.*, *Appl. Phys. Lett.* **89**, (Jul, 2006).
108. J. Biener *et al.*, *Nano Lett.* **6**, 2379 (Oct, 2006).
109. A. M. Hodge, J. R. Hayes, J. A. Caro, J. Biener, A. V. Hamza, *Adv. Eng. Mater.* **8**, 853 (Sep, 2006).
110. A. S. Dalton, E. G. Seebauer, *Surf. Sci.* **601**, 728 (Feb, 2007).
111. E. G. Seebauer, C. E. Allen, *Prog. Surf. Sci.* **49**, 265 (Jul, 1995).
112. R. G. Gordon, D. Hausmann, E. Kim, J. Shepard, *Chemical Vapor Deposition* **9**, 73 (Mar, 2003).
113. J. Kirn, E. Samano, B. E. Koel, *Surf. Sci.* **600**, 4622 (Oct, 2006).
114. R. Zeis, A. Mathur, G. Fritz, J. Lee, J. Erlebacher, *J. Power Sources* **165**, 65 (Feb, 2007).
115. M. Chen, Y. Cai, Z. Yan, D. W. Goodman, *J. Am. Chem. Soc.* **128**, 6341 (May, 2006).

116. M. S. Chen, D. W. Goodman, *Science* **306**, 252 (Oct, 2004).
117. K. Kamata *et al.*, *Science* **300**, 964 (May, 2003).
118. M. Jakob, H. Levanon, P. V. Kamat, *Nano Lett.* **3**, 353 (Mar, 2003).
119. E. W. McFarland, J. Tang, *Nature* **421**, 616 (Feb, 2003).
120. J. A. Rodriguez *et al.*, *Science* **318**, 1757 (Dec, 2007).
121. S. Ghosal *et al.*, *Chem. Mat.* **21**, 1989 (May, 2009).
122. S. O. Kucheyev *et al.*, *Langmuir* **24**, 943 (Feb, 2008).
123. J. Biener *et al.*, *Nanotechnology* **18**, (Feb, 2007).
124. S. O. Kucheyev *et al.*, *Appl. Phys. Lett.* **86**, (Feb, 2005).
125. J. S. King *et al.*, *Nano Lett.* **8**, 2405 (Aug, 2008).

Curriculum Vitae

Arne Wittstock

Personal data

- Born in Bremen (Germany), March 14th, 1981.
- Address: Institute of Applied and Physical Chemistry, University Bremen, Leobener Str. NW2, 28359 Bremen, Germany
- E-mail: awittstock@uni-bremen.de

Education

- 2006: Diploma in Chemistry (Dipl.-Chem.), summa cum laude (1.0), University Bremen, Germany
- 2000: Abitur, Altes Gymnasium in Bremen (1.3)

Work experience

- since 2006: PhD Study at the Institute for Applied an Physical Chemistry at the University Bremen, Germany
- 2006: Research assistant, Krüss GmbH, Hamburg, Germany (Diploma thesis)
- 2003 - 2006: Teaching assistant at the University Bremen (mathematics, physical chemistry, and lab training).
- 2002 – 2005: Software development (C++) at the MIR Chem GmbH, Bremen, Germany

---

Research visits

- 2007 - 2008: Research stay at the Lawrence Livermore National Laboratory, Livermore, USA
  (Dr. Alex Hamza).

.

Research Interests

Chemistry of surfaces, physical chemistry and surface reactions at nanostructured surfaces, catalytic studies under ambient conditions, innovative catalyst materials (such as nanoporous foams)

Publications

(1) Wittstock, A., Zielasek, V., Biener, J., Friend, C. M. & Baumer, M.; Nanoporous Gold Catalysts for Selective Gas-Phase Oxidative Coupling of Methanol at Low Temperature; *Science* 327, 319-322, doi:10.1126/science.1183591 (2010).

(2) Wittstock, A.; Neumann, B.; Schaefer, A.; Dumbuya, K.; Kübel, C.; Biener, M. M.; Zielasek, V.; Steinrück, H.-P.; Gottfried, J. M.; Biener, J.; Hamza, A.; Bäumer, M.; Nanoporous Au: An Unsupported Pure Gold Catalyst?; *The Journal of Physical Chemistry C* **113**, 5593-5600, doi:doi:10.1021/jp808185v (2009).

(3) Biener, J.; Wittstock, A.; Zepeda-Ruiz, L. A.; Biener, M. M.; Zielasek, V.; Kramer, D.; Viswanath, R. N.; Weissmuller, J.; Bäumer, M.; Hamza, A. V.; Surface-chemistry-driven actuation in nanoporous gold; *Nature Materials* **8**, 47-51, doi:10.1038/nmat2335 (2009).

(4) Biener, J.; Wittstock, A.; Baumann, T.; Weissmüller, J.; Bäumer, M.; Hamza, A.; Surface Chemistry in Nanoscale Materials; *Materials* **71**, 603-612 (2009).

(5) King, J. S.; Wittstock, A.; Biener, J.; Kucheyev, S. O.; Wang, Y. M.; Baumann, T. F.; Giri, S. K.; Hamza, A. V.; Baeumer, M.; Bent, S. F. *Nano Lett.* **8**, 2405-2409, doi:10.1021/nl801299z (2008).

(6) Hass, E. C.; Ottensmeyer, R.; Wittstock, A.; Foam characterization by optical measuring techniques and computer-aided image processing; *Tech. Mess.* **71**, 603-612 (2004)

Patents

[I] ACTUATION VIA SURFACE CHEMISTRY INDUCED SURFACE STRESS, IPC8 Class: AC23C2200FI, USPC Class: 148240, Status: pending

[II] METHOD AND DEVICE FOR MEASURING FOAM**,** WO/2005/003758, international Filing Date: 24/06/2004